Preservation strategies for a monument affected by Mg-sulfate salts: the cloister from El Paular Monastery, Madrid, Spain

Abstract

The cloister from El Paular Monastery is highly affected by salt crystallization of Mg-sulfates and presence of chlorides and nitrates. In order to avoid salt crystallization, the consequent deterioration of building materials and to keep the stability of some significant paintings that will be exposed inside the cloister, after the characterization of building materials and salts, three preservation strategies has been established based on architectural, pethophysical and physical-chemical features.

The main source of Mg-sulfate salts is the high concentration of moisture and raising damp by capillarity, especially through the mortars which are the most porous materials. The dissolution of gypsum (Ca-sulfate) as component of the mortars and its interaction with magnesium from the mortars, granite and dolostone give rise to Mg-sulfates that migrate through the porous building materials. The installation of a ventilation system would avoid the rising damp and hence the dissolution, mobilization and crystallization of salts. The salt reduction of building materials have been performed with cellulose poultices with pores between 15-20 μm and between 10 and 30 μm diameter. The monomodal distribution and smaller pores of dolostone (1 and 3 μm) and mortars (0.1 and 10 μm) is the cause of the lesser effectiveness of salt reduction in these materials compared to the granite, with a polymodal pore size distribution and pores distributed in the range 100-300 μm. A higher number of cellulose poultice applications could increase the efficiency of this desalination procedure. However, there is no a warrantee of the total extraction of salts and the mixture of this cellulose poultice with clays to shift the PSD to smaller sizes would be more efficient to desalinate dolostone or mortar. The most suitable environmental conditions, inferred from thermodynamic model predictions (Runsalt software) and experimental work based on relative humidity transfer inside the stone, predict that to avoid salt crystallization these values would be 17º±2ºC and 55±2% RH.

However, if there are some failures in the ventilation system or in the environmental control we recommend keeping the paintings to be exposed on the walls of the cloister inside glass cases. This research represents both a practical and experimental work useful for conservation scientists and restorers involved in the field of preservation of monuments and environmental impact to avoid salt crystallization.

Keywords Mg-sulfate salts · building materials · salt crystallization · preservation strategies · environmental control.

Introduction

In Spain, the most important Carthusian monasteries were those from Scala Dei in Tarragona, Miraflores in Burgos, Portaceli in Valladolid and El Paular in Madrid. The latter is founded in 1086 AD and undergoes several restoration works. The first significant interventions were in the period 1440-1486 AD, when the main cloister and other areas were restored. Other main intervention period was between 16th and 18th centuries. The cloister was mostly reconstructed reusing the materials from the former cloister.

In the excavations of the gardens of the East hallway of the main cloister, more than 50 stone structures with ornamentation of abandoned nobles' parts and used as refilling material were found. In 1835, the disentailment and secularization decree put the end of the monastic life. The monastery and its properties

were given to the Spanish State who transferred it to private owners. From that time, the building started to deteriorate, until to become almost as ruins in a few time. In 1874, the Spanish state acquired the areas of the monastery with higher architectonic value. In 1876, the monastery was declared Historical-Artistic Monument. The main restorations were performed only in those areas with the most necessary urgent interventions. Between 1887 and 1890 the vaults and the roofs were repaired. In 1918 a higher restoration work of those areas that required the most immediate interventions was performed. The main cloister, the 18th century courtyard, the church and other areas were restored. After the civil war, the restoration works continued on the different walls, vaults and roofs, church and cloister. In the period 1953 and 1973 the restoration work continued affecting the main cloister in 1958, 1961 and 1963. Between 1975 and 1980 the restoration works were mainly focused on the roofs from the cloister and church. The most radical changes carried out in the monastery have taken place during the 17th century with the introduction of the granite stone and later with the restoration works during the 20th century.

Currently, SOPSA, S.A. architectural company is in charge of the restoration and conservation works in the main cloister of the monastery. This intervention, together with those already performed and those still to be perform partially belong to the Director Plan of Restoration that the Ministry of Culture and Madrid Region. It started in 1987 and is coordinated by the architect Eduardo Barceló de Torres.

These restoration works are designed to fit out the galleries of the cloister for a permanent exposition of Vicente Carducho paintings. One of the main concerns is the stability of these significant paintings since they will be exposed in the cloister where the crystallization of salts should be avoided.

In 1996 a research project carried out by López-Acevedo et al. to study the main weathering patterns in the cloister of El Paular Monastery concluded that the stone decay was mainly caused by the combination of humidity and soluble salts. These authors found that the main salts efflorescences were magnesium sulfates and that the jointing mortars had gypsum in their composition.

Magnesium sulfate is considered a very destructive salt that plays an important role in the deterioration of stone (Shaffer RJ 1932; Charola and Lewin 1979; Cooke and Gibbs 1991; López-Arce et al. 2008). The original source of magnesium present in magnesium sulfate efflorescence is generally tied to be the composition of the building materials used for construction, mainly dolomite or magnesium limestone (Shaffer RJ 1932; Caner et al. 1985; La Iglesia et al. 1994; Villegas et al. 1996) as well as magnesium-rich mortars (Lauri et al. 1925; Charola and Lewin 1979; Klemm and Siedel 1996; González-Limon and Buergo Ballester 2002; Tulliani et al. 2005; López-Arce et al. 2009a).

Mortars made by mixing lime and gypsum have been used very often during the 17th, to 19th centuries, for wall and joints restorations and as stuccos or plasters over the stone surface, and occasionally were also made of pure gypsum (Chiari et al. 1992). The binder fraction of ancient mortar samples from five Italian Churches from Northern Italy was analyzed by Bruni et al. (Bruni et al. 1998) and they found three different species of lime composed of: (i) calcareous lime with only calcite, in the bedding or jointing mortars (15th century) for brick masonry, (ii) magnesium lime with calcite and magnesite, in the painted plasters (15th century), and (iii) magnesium lime with calcite and magnesite and hydromagnesite in the exterior plasters covering the masonries (6th-7th, 15th and 17th centuries).

A clear example of incompatibility of some building materials was found in other monastery from Spain, where the combination of sulfate-bearing mortars and magnesium-rich stone and mortars leaded to extensive weathering by magnesium sulfate crystallization (López-Arce et al. 2009a).

The aim of this work is to establish preservation strategies on El Paular Monastery based on architectural, pethophysical and physical-chemical features. In order to do that: i) the characterization of building materials and salts was carried out to determine the decay, and ii) the salt reduction of building materials was performed and the efficiency of the procedure was evaluated. Finally, the most suitable environmental conditions were inferred from thermodynamic model predictions and experimental work

on the study of relative humidity transfer inside the stone simulating summer and winter conditions inside the cloister.

Materials and Methods

The monastery is located in the Northwest of the Region of Madrid, about 100 km from the City Centre. The construction of Santa María de El Paular monastery was mainly built with stone masonry. In many areas there are also walls built with bricks. The work carried out in this research is mainly focused in the cloister of the monastery (Fig.1).

Currently, granite stone is the main building material located in the basement (1 m high) and in the outer walls of the building. Originally, dolostone was used in the outer walls, but after the several restorations it was used in the indoor walls above the granite basement, in the nerves and keystone of the crypt. There are jointing and plaster mortars. The former, are located between bricks and stone masonry. The latter, are located mainly in the indoor walls built with dolostone. In some areas it is detached from the surface and in other areas several layers of this plaster mortar can be observed.

Sample materials collection

Figure 1 shows the map of the cloister and the areas of sampling (stone, bricks, mortars and salts).

Stone samples

Seven samples of granite stone have been collected from the cloister (samples G1 to G7). Fifteen samples of fragments of dolostone were collected (samples D1 to D15), from the indoor walls of the rooms attached to the cloister (Fig.1). Sample of dolostone D11 have been selected to conduct an experimental work to study the relative humidity transfer though the stone exposed at different relative humidity conditions simulating summer (30ºC) and winter (3ºC) seasons inside the cloister.

Mortar samples

Twenty five jointing (MJ) and plaster (MP) mortar samples have been taken. Seven samples (MJ3, MP4, MP5, MJ6, MJ8 and MP18 where collected from the indoor walls of a room behind the West hallway. Sample MP7 was taken from the outer stone masonry of this room and MJ8 was taking form the joints of a brick indoor wall. Eighteen mortars were collected from the cloister, ten jointing mortars (MJ1, MJ2, MJ9, MJ10, MJ19, MJ20 and MJ22 to MJ25) and three plaster mortars (MP16, MP17, MP21). Samples MJ11 to MJ15 belong to buried samples located under the granite pavement where ancient structures made of brick and stone where discovered (Fig.1).

Salt samples

Three salt efflorescence samples were collected from the Northwest corner of the inner wall of the North hallway of the cloister (samples S1, S2 and S3). The samples were located on the surface of the dolostone wall and on the nerve of the crypt.

According to the study of salts efflorescences carried out on the cloister of this monastery by López-Acevedo et al. (1996), the North hallway of the cloister was the area with the highest decay (highest amounts and different types of salts). Furthermore, in this area there are significant humidity and temperature changes since it is located very close to the access of the cloister entrance. For this reason, the corner of the inner wall of the North hallway has been selected for the drilling of materials at different heights and depths. The extracted powder was then analyzed by ion chromatography to determine the type and concentration of soluble salts present in the drilled materials.

Twenty drillings have been performed (Fig.2) in the stone (granite and dolostone), jointing mortars and bricks, at different heights (every 70 cm from the bottom of the basement to the top of the roof) and at different depths (at 0.5 cm, 1cm, 1.5 cm, 3cm and 5 cm from the surface of the drilled materials).

This area was also selected for desalination with a cellulose poultice ARBOCEL Bxx supplied by CTS, since it is one of the most often type of poultice used in the field as desalination material. Three drillings were selected to asses its efficiency: one drill on the granite from the basement (2 cm high; sample DG1), one drill from a dolostone (2.10 m high; sample DD7) and one drill from a jointing mortar (2.10 m high; sample DM8). These drilled samples were selected to measure the soluble salts by ion chromatography at the different indicated depths before and after poulticing. Five applications of this poultice were performed. After each application, and before the poultice was completely dried, this was removed and the soluble salts and conductivity values were measured

Methods for materials characterization

X ray Diffraction analyses were performed on the powder fraction of total sample with a PHILIPS PW 1752 powder diffractometer with CuKa radiation. Patterns were obtained by step scanning from 2º to 68º 2θ with a scan step size of 0.02° and 2º/min in a continuous mode. The working conditions were 40kV and 30 mÅ. PC-ADP Diffraction Software and Difract AT, version EVA V 3.2 were used to obtain the diffraction patterns and for mineralogical phase identification.

Environmental Scanning Electron Microscopy (ESEM) was performed to study the morphology and composition of stone, mortars and salts using a Quanta 200 FEI microscope with Energy Dispersive X-ray Spectroscopy (EDS) (model 7509 Oxford Instrument Analytical, UK).

Polarized light optical microscopy was performed to study the surface sections of the stone and mortar samples to characterize the mineralogy and the physical-chemical weathering patterns. Thin sections of stone were studied with an Olympus BX51 polarized light microscope fitted with an Olympus DP 12 (6V/2,5Å) digital camera and proprietary software.

Water absorption under vacuum was performed to determine the bulk density, open porosity and to quantify the amount of water absorbed by the specimens once they reach saturation, as described in the Spanish and European standard UNE-EN 1936: 2006 on natural stone test methods. Water absorption by capillarity and at atmospheric pressure was made according standard test UNE-EN 1925:1999 and UNE-EN 13755:2002, respectively.

Propagation of ultrasound velocity was measured for Vp (P-wave velocity) that is related to effective porosity. P-wave propagation time was measured to a precision of 0.1μs with a PUNDIT CNS Electronics instrument. Standard recommendations were followed according to Spanish and European standard UNE-EN 14579: 2005 The frequency of the transducers used was 54 KHz. Measurements were taken in direct transmission/reception mode, across opposite parallel sides of the cubic specimens in all three spatial directions.

Mercury intrusion porosimetry (MIP) was measured to asses sample pore structure, i.e., connected or open porosity (P) and pore size distribution (PSD). Readings were taken in pore diameters of 0.005 to 400 μm under measuring conditions ranging from atmospheric pressure to 60,000 psia (228 MPa). Sample cores 10 mm in diameter and at least 30 mm high were cut and analyzed with a Micromeritics Autopore IV 9500 MIP.

Drilled powder samples collected at the depths and heights mentioned above were taken with an electrical drilling device fitted with a 0.8 cm diameter bit.

Ion Chromatography was performed to identify the soluble salts on all the drilled materials before poulticing. After poulticing, only the three materials selected and described above were analyzed. The

concentration of soluble salts was also measured in the poultice used for desalination. The samples (0.1 g aprox.) were dissolved in 10 ml of MiliQ water and introduced 45 min in an ultrasonic bath (Selecta model Ultrasounds-H) at 60ºC and centrifuged with a Heareaus Thermo model Labofuge 400 during 2 min, at 3500 rev/min a centrifugous forze of 3400 rfc. After sample extraction, the quantification of soluble salts (anions and cations) was carried out with a Metrohm 761 Compact IC ion chromatograph.

The quantitative results of soluble salts obtained with ion chromatography were analyzed according to a chemometric model used to identify correlations between quantified cations and anions with VisualMinteq 2.61 software. A thermodynamic model was then carried out with RUNSALT software 1.9 which is a version of ECOS software (Price 2000) that is based on the Pitzer theory of electrolyte solutions (Pitzer 1973). This software predicts the phase minerals which are present in equilibrium at a certain relative humidity and temperature. The charge balance of anions and cations has been manually performed since the autobalance facility of this software can give misinterpretation of the data. The prediction of gypsum crystallization might cause problems, since the software is unable to calculate the crystallization of other salts in its presence. For this reason it has been removed from the system. Several models were performed with the RUNSALT software changing the environmental conditions to simulate the average temperature during summer (30ºC) and winter (3ºC) seasons. The relative humidity (RH) ranging between 30% and 90% has been considered in both cases. The models were applied using the ion chromatography results obtained at the most superficial drill (0.5 cm) of the selected granite (DG1) and mortar (DM8) before and after desalination with poultices. In the case of dolostone (DD7) all the ion chromatography results obtained at the different depths (0.5, 1, 1.5, 3 and 5 cm), before and after desalination, were introduced in the model since this is the most abundant type of stone in the monastery. In order to predict the most suitable environmental conditions to avoid salt crystallization in the stone from the cloister, several temperatures (3º, 10º, 15º and 20ºC) together with the results obtained at the different depths of DD7 sample after desalination were introduced in the software.

As was mentioned above a dolostone sample (D11) was selected for an experimental work to study the humidity transfer though the stone exposed at different relative humidity conditions simulating summer and winter seasons in the cloister. Environmental control devices to measure temperature a relative humidity (I-buttoms ref) with a round shape of 2 cm diameter and 0.5 cm thick where introduced at 1 cm, 3 cm and 5 cm from the surface of the dolostone sample. Two sub-samples of dolostone D11 were selected to be introduced in desiccators used a climatic chambers. The equilibrium relative humidity (RHeq) of specific supersaturated salt solutions was used to keep the humidity constant at 20ºC: $MgSO_4$ (RHeq 90%) to simulate a very humid environment, NaCl (RHeq 75%) to simulate a humid environment and $Mg(NO_3)_2$ (RHeq 54%) to simulate a dry environment.

A stone sub-sample with a natural crust on the surface and other without this crust were drilled in order to introduce the i-buttoms at the different mentioned depths. Then, the samples were covered with a parafilm layer and a thermo insulator poly-propylene layer in all the faces except one of them. A reference i-buttom was used as blank to record the T and RH conditions outside the samples. First, the samples were introduced first in the chamber at 54% RH and placed in the stove at 30ºC during 1 week. Then, these were transferred to the chambers at 75% RH and left again in the stove at the same temperature and time. After one more week, the samples at 75% RH were placed in the freezer at 3ºC during 1 week and then transferred to the chambers at 90% RH at the same temperature during 1 last week. Finally, the same procedure was applied in the opposite order to register the same conditions but this time from higher to lower HR and from lower to higher temperatures.

Results and discussion

Materials characterization and conservation state

The main weathering patterns observed in the granite stone is the color alteration, loss of cohesion, disaggregation and detaching of surface layers. The dolostone is mainly weathered in the nerves of the

crypt with loss of material, being necessary the replacement of the stone in some areas. The jointing mortars display cracks and loss of material mainly between dolostone blocks. The plaster mortars have been detached from the surface of the stone where they have been applied. The bricks show powdering and loss of material processes. All these building materials are affected by salt efflorescences, especially the dolostone, which give rise to believe that these salts can be also inside these materials.

Granite samples

The granite samples, both from the basement and the pavement of the cloister display similar petrographical and mineralogical characteristics. They correspond to a monzogranite with coarse to medium grain with more or less biotite that in some samples is oxidized giving rise to a brownish-orange discoloration of the granite. The main mineralogy is quartz, feldspar (orthoclase and plagioclase) and biotite (Fig.3a), with zircon and apatite as accessory minerals and sericite, epidote, muscovite and chlorite as weathering minerals. The granite samples from the pavement display more cracks and fissures being more weathered than those from the basement. The granite samples from the pavement display a differential weathering between inner and outer areas of the samples (Fig.3a-3d). In the outer areas, the quartz and plagioclase are fissured. This allows the water to be introduced through the stone, being responsible of the hydraulic reactions that cause the sericitization and kaolinitization of plagioclases, favoring decohesion of the stone and the oxidation of the biotites (Fig. 3b).

The average ultrasound velocity values (Vp) shows that these are lower in the outer or more superficial areas of the granite sample (G1) compared to their inner areas (Vp = 1317 vs. 1684 m/s), with higher values of open porosity accessible to water (Φw = 5.16 vs. 4.79%) and accessible to mercury (ΦHg = 5.67 vs. 4.92%) and saturation (S = 2.07 vs. 1.92%). The coefficient of water absorption is also higher, measured both at atmospheric pressure (Ca = 1.75 vs. 1.65%) and by capillarity (Cc = 24.22 vs. 21.13 $gr/m^2 \bullet s^{1/2}$). The mercury intrusion porosimetry values obtained in the granite samples from the basement (G7) show a low total porosity (ΦHg = 2.68%), even lower compared with the inner area of the granite sample (G1) from the pavement (ΦHg = 4.92%). The PDS shows a polymodal curve in both samples, with the highest number of pores distributed in the range between 10 and 100 μm of diameter. The inner area of granite from the pavement (G1) shows very similar PDS (Fig.3c) to the outer area of this sample (Fig. 3d). However, the outer area displays the development of pores with sizes below 0.01 μm and the increase of pores with a diameter in the range 100-300 μm (Fig. 3d).

Taking into account the long time exposure (since 17th century) of the granite samples from the pavement to water uptake from underground, if we compare the petrophysical characterization values with those obtained in similar fresh granite samples from Madrid Region (López-Arce et al. 2010) it can be considered that they have a bad conservation state.

Dolostone samples

The most abundant dolostone type in the building is a dolopelmicrite (sample D1). It displays a homogeneous and compact aspect, abundant pellets, quartz grains (30 μm) embedded in the equigranular dolomite crystal (< 4 μm of diameter) matrix and intense bioturbation (Fig.3e). The other dolostone type is a dolobiomicrite (sample D2). It is more heterogeneous; with significant non cemented porosity, displaying fewer amounts of pellets, no quartz, dolomite crystals with higher amount of calcite compared with the former dolostone (Fig. 3f). Pores of 1 mm diameter can be macroscopically observed and apparently seems that it has a higher amount of porosity compared to the dolopelmicrite stone.

However, mercury intrusion porosimetry analyses performed on the dolobiomicrite stone give a lower value of total porosity (ΦHg = 24.12%) compared to the higher value (ΦHg = 30.96%) obtained on the dolopelmicrite stone, which also has a higher amount of micropores < 5 μm (98.3 vs. 37.6%). Fig. 3g and Fig. 3h show the PDS of both types of dolostone, with the highest amount of pores distributed in the

range between 1 and 3 μm of diameter in the dolopelmicrite stone and between 10 in 30 μm in the dolobiomicrite stone.

The petrophysical characterization was carried out in the most abundant dolostone present in the cloister of the monastery (dolopelmicrite). It shows an average ultrasound velocity values that range between 3100 and 3350 m/s. The open porosity accessible to water is Φw = 30% and accessible to mercury is ΦHg = 30.96% and saturation S = 7.49%. The coefficient values of water absorption measured both at atmospheric pressure and by capillarity are Ca = 13.47% and Cc = 182.06 $g/m^2 \cdot s^{1/2}$ respectively. Salt weathering quantified by the percentage of weight loss after salt crystallization has a dependence on the petrophysical properties of the material (Benavente 2007). The influence of anisotropy on the durability of a similar type of dolostone has been studied by Fort et al. 2008 showing that salt crystallization processes are significantly affected by petrophysical properties that also depend on the anisotropy of these rocks. The total porosity and PDS exert a significant influence on the hydrical behavior of the stones. In the dolostone, the higher total porosity and the monomodal or bymodal PDS concentrated between 0.1 and 3 μm give rise to faster water absorption with a higher coefficient by capillarity than in the granite stone with a lower total porosity and polymodal distribution concentrated between 10 and 300 μm. These results indicate that dolostone has a higher potential to deteriorate compared to the granite, because pores with smaller sizes are more susceptible to the weathering action caused by water and salts. Materials with high porosity, small pores and low strength are more prone to salt weathering (Benavente et al 2003; Benavente et al 2004).

Mortar samples

The XRD and optical microscopy results obtained in the jointing mortars from the cloister show a composition of the aggregates formed by quartz, potassium feldspar, plagioclase and biotite. The binder is mainly calcite and dolomite which indicates an original binder composition of lime (CaO) and magnesia (MgO). These dolomitic mortars were manufactured from burning dolostone; probably the same type than those present in the cloister. Table 1 shows the XRD results of all the collected and analyzed mortar samples. Some clay was also identified, which provenance could be from the aggregates that were not properly washed before the manufacture of the mortars. Most of the analyzed mortars display also magnesium sulfate salt (epsomite, $MgSO_4 \cdot 7H_2O$). The binder usually displays gypsum, both in the plaster and jointing mortars. The plaster mortars collected from the walls of the cloister are mainly gypsum. Fig.4a shows the ESEM image of the plaster mortar (MP17), where signs of dissolution and microporosity can be observed. The XRD results show that the external layer of this sample displays mainly gypsum, calcite and quartz (Fig.4b). The inner layer of this sample displays calcite, dolomite and other minerals from the aggregates and epsomite salt. The ESEM-EDS and XRD results also show the presence of hydromagnesite in jointing mortar sample MJ7 (Fig. 4c and 4d). Hydromagnesite has also been identified in calcitic and magnesian limes from sculptures located in a funerary crypt with a permanent dampness and constant water seepage environment (Villaseñor and Price 2008). These authors found a relationship between the crystallization of hydromagnesite and the high shrinkage observed in the materials due to dehydration of hydrated magnesium carbonates. In our samples, besides hydromagnesite it has also been observed signs of dissolution and re-precipitation of silicates and calcium-magnesium aluminosilcates, probably due to hydraulic reactions between the clays and the carbonates. The binder of the jointing mortars also displays nodules (0.2-1 cm of diameter) with a high proportion of magnesium. In some jointing mortar samples there is presence of sulfur, calcium, magnesium, sodium and chloride. The EDS mappings have allowed localizing the distribution of these elements in the samples (Fig. 5). These results seem to indicate the presence of calcium sulfate (Fig.5b and Fig. 5c), magnesium sulfate and sodium chloride (Fig. 5e and Fig. 5f). The presence of potassium in these areas has also been identified, which could correspond to potassium nitrate.

The gypsum, although is present in low amounts and only in some samples, could has been a key component in the mortars and in the precipitation of soluble salts. The transformation of gypsum into calcite due to infiltrations of carbonated solutions (Fernández-Díaz et al. 2009) could be the cause of the

low quantities of gypsum detected in the mortar samples and the massive precipitation of the sulfate salts. The high humidity and the capillarity rising in the cloister could have caused the dissolution of the mortars, the transformation of gypsum into calcite, the migration of sulfates and the final recombination with the high magnesium amount present in the stone (dolostone and granite) and dolomitic mortars. The final products are the soluble magnesium sulfate salts that can easily circulate through the porous building materials, especially through the mortars. The higher microporosity (20% between 0.01-0.1μm and the high surface area of the jointing mortars from the pavement of the cloister, highly affected by damp, could be a sign of these processes.

The environmental fluctuations that cause the crystallization-dissolution and hydration-dehydration of these hygroscopic salts inside the pore materials could also have played an important role in the weathering processes of the building materials giving rise to their lamination, disaggregation and disintegration.

The total porosity of these mortars is very high (40%), and is mainly localized in the pores with a diameter in the range 0.1-10 μm. The main difference in the PDS of jointing and plaster mortars (Fig. 4e and Fig. 4f) is that plaster mortars display a polymodal distribution curve with pores distributed in three ranges 0.1 and 1 μm, 1 and 10 μm and 10 and 100 μm. Their pores are mainly distributed in the range 0.1 and 10 μm. However, jointing mortars display a bymodal distribution with pores in the ranges 0.1 - 1 μm and 1 – 10 μm, with their pores mainly distributed in this latter range (Fig. 4e).

Salt samples

The XRD results show that the main salt efflorescences found in the building materials from the cloister are calcium and magnesium sulfates (gypsum ($CaSO_4 \cdot 2H_2O$), epsomite ($MgSO_4 \cdot 7H_2O$) and hexahydrate ($MgSO_4 \cdot 6H_2O$)).

The ion chromatography results show that the main anions analyzed in the stone, bricks and mortar samples are nitrates and sulfates, although small amounts of chlorides were also identified. The mortar samples are the building materials with the highest amounts of sulfates and nitrates (Fig.6).

In the granite drillings and in the adjacent jointing mortars located at 2cm and 70 cm from the basement (Fig. 2 and Fig. 6), the sulfate and nitrates content decreases with height and with depth. In the dolostone drillings, the ion chromatography results obtained in the samples located at 1.40 m and 2.10 m from the bottom of the basement show that also the amount of sulfates decreases with height and depth. However, the amount of nitrates decreases with height but increases with depth.

The amount of sulfates ranges between 0.43 and 111.26 mg/l in granites, between 1.22 and 235.97 mg/l in mortars, between 1.17 and 78.36 mg/l in dolostone and between 1.64 and 117.82 mg/l in the bricks. The amount of nitrate ranges between 0.62 and 3.42 mg/l in granites, between 0.1 and 28.54 mg/l in mortars, between 0.7 and 3.11 mg/l in dolostone, and between 0.51 and 6.23 mg/l in bricks. In all the drillings have been detected also the presence of fluorides, chlorides and nitrites. However, these salts are present in very scarce proportion (between 0.08 and 0.70 mg/l). In some drillings performed in mortar the amount of chlorides is slightly higher (between 1.00 and 5.00 mg/l). Fig. 6e and Fig. 6f show the distribution of chlorides in the stone, bricks and mortars. It can be observed that the highest amount of chlorides in the stone is found at the surface of the granite and at higher depths in the bricks (Fig. 2 and Fig. 6e). In the mortars the highest amount of chlorides is located close to the adjacent samples mentioned above and at the surface of the wall decreasing with depth.

The fact that the amount of sulfates in the dolostone decreases with height and with depth could be related with a contribution of sulfates from the basement and from the surface of the wall. Additionally, there is a contribution of salts from filtrations from the roof (where the bricks are located). The presence of gypsum in some mortars collected under the pavement is an indication of the higher quantities of sulfates at lower heights. The high quantities of gypsum present as the main component in the plaster mortars also explain

the higher amounts of sulfates on the surface of the wall. In the mortar samples, the decrease of amount of nitrates with height but its increase with depth indicates that these salts come from the soil. The amount of sulfates, both in stone and bricks, generally decreases down to a depth of 5 cm. However, in the bricks the amount of chlorides and nitrates increases with depth.

Therefore, the source of these sulfate salts seems to be the gypsum used in the plaster mortars. The source of nitrates could be the soil from the underground that could be used in the past as fertilizer or from organic excrements (Viles and Goudi 2007). The bird excrements could also explain the high amount of nitrates and chlorides found at the roof (Gómez-Heras et al. 2004).

As was mentioned above, the main source of magnesium sulfate salts seems to be the high concentration of moisture and the raising damp by capillarity, especially through the most porous materials, the mortars. The dissolution of gypsum (calcium sulfate) as component of the mortars and the interaction with magnesium also from the mortars, granite and dolostone can easily precipitate magnesium sulfates that migrate through the porous building materials. The anionic migration ($SO_4^{=}$), also due to carbonation of gypsum (Fernández-Díaz et al. 2009), and the cationic (Ca^{2+}-Mg^{2+}) recombination, taking place mainly in and through the mortars (with higher amount of magnesium) seems to be the cause of the massive precipitation of magnesium sulfates. Similar cases have been found in other monasteries in Spain, built with similar building materials and probably re-used during restoration work (López-Arce et al 2009a).

The presence at the same time of magnesium sulfate salts with different states of hydration indicates the influence of humidity and temperature fluctuations inside the cloister. Fig. 7a shows the XRD pattern of a salt efflorescences sample collected from the surface of a dolostone. It display the presence of both, epsomite ($MgSO_4 \cdot 7H_2O$) and hexahydrite ($MgSO_4 \cdot 6H_2O$) salts together with dolomite, probably from fragments detached during the efflorescence rising. The ESEM image (Fig.7b) show these magnesium sulfate crystals where the hydration state of epsomite can be inferred from the smooth surface of the crystals while the dehydration state of hexahydrite it follows from the rough appearance.

Preservation Strategies

In order to solve the salt crystallization process and the consequent deterioration of building materials inside the cloister, after a first diagnostic or characterization of building materials and salts, we have established three preservation strategies based on architectural, pethophysical and physical-chemical features: i) *installation of a ventilation system*, ii) *salt reduction of building materials* and efficiency evaluation, and iii) *determination of the most suitable environmental conditions*, inferred from thermodynamic model predictions and experimental work based on relative humidity transfer inside the stone.

Ventilation system installation

Maintaining underfloor ventilation is an important part of controlling damp, as it allows ever-present soil moisture to evaporate beneath the floor and to pass out through the vents in the base of the walls. The moisture 'stress' on the walls would be much greater without this ventilation (Young 2008). The ventilation system designed for the cloister consists in two underfloor ventilation channels, attached to the walls, under the granitic pavement covering the whole perimeter of the cloister. A third ventilation channel is located attached to the external wall, outdoors of the building. These channels, located along the perimeter of the indoor cloister and outdoor building, have 60 cm wide and 50 cm height. The two ventilation channels inside the cloister are communicated between them through plastic top slabs that are supported over a concrete pavement with a base of clean boulder fragments. Natural ventilation is achieved due to the total ventilation through the holes drilled in the outdoor wall that communicate with the ventilation channels from the walls and pavement of the cloister. Similar ventilation systems have been installed in buildings with harsh problems of rising damp and salt attack in the city of Adelaide located in South Australia (Young 2008; López-Arce 2009b). Controlling evaporation of moisture from

sub-floor walls or from adjacent soils is one of the fundamentals of successfully managing rising damp. Although, too much underfloor ventilation may lead to salt attack on the inside faces of walls and on dwarf walls supporting floors. This could lead to unseen damage and could become dangerous. Regular inspection of underfloor spaces is therefore important.

Furthermore, it has been built a forced ventilation system that consists in some probes located inside the cloister that activate the ventilation funs located outdoors. These funs introduce air into the cloister as a function of the real humidity and temperature conditions inside the cloister and of those previously programmed to be the most stable conditions. These suitable conditions are based on the thermodynamic model predictions and the experimental work on relative humidity transfer inside the stone.

Salt reduction from building materials

As was mentioned above, one of the main deterioration processes that affect the building materials from the cloister is the presence of soluble salts. From the XRD results carried out on salts efflorescences and mortar samples, it can be stated that the main salt is epsomite. The solubility of this salt is quite high (71 gr/100 ml at 20ºC) and is easily dissolved if the relative humidity is higher than 90%. The ion chromatography results show that the highest amount of sulfates and nitrates are preferentially located at 0.5 cm from the surface of the building materials. The mortars are the materials with the highest amounts of these salts mainly due to their higher porosity. For this reason, is necessary to proceed to get rid of these salts, in spite of this is a difficult task and frequently is not possible the total desalination from building materials.

Before the salt reduction process with poultices, the surface of the building materials was brushed to remove the salt efflorescences. During brushing the detached particles were absorbed with an aspiration device to avoid the deposition of these particles in other areas. The cellulose poultice has been tried on the same area where the previous drilling of building materials was performed. Five applications of poultices were carried out on the three selected drillings (Dg1, DD7 and DM8 shown in Fig.2 and Fig. 6)) to asses its efficiency through ion chromatography and conductivity measurements (Table 2). The conductivity of the soluble salts leached from the poultices applied on the different building materials decreases after each application, especially in the granite sample. This is in agreement with the ion chromatography results of the soluble salts leached from the poultices. The granite stone is the material with highest salt absorption by the poultices, with a conductivity decrease circa 70%. The conductivity and the soluble salts measurements from the poultices applied on the mortars also decrease (circa 50%), except the chlorides and nitrites salts. In the case of poultices applied on the dolostone, the conductivity decreases (circa 46%) and the nitrites and nitrates as well. However, sulfates and chlorides extraction increases after each poultice application.

The ion chromatography results made on the soluble salts from the second drillings performed on granite (DG1), dolostone (DD7) and mortar (DM8), show that the amount of sulfates and nitrates after the application of poultices are significantly reduced, especially in the granite and in the mortar (Fig.8). In the dolostone, the amount of nitrates is slightly reduced and the amount of sulfates is reduced up to 1cm, but increases at 1.5 and 3 cm from the surface.

After poulticing, the amount of chlorides is increased at all the analyzed depths in the three types of materials, except in the surface (0.5cm) of the granite. The amount of chlorides seems to increase especially in the surface of the mortars. On the research carried out by Bourgès and Vergès-Belmin (2008) on desalination of limestone with different types of poultices these authors observed that the cellulose poultice caused a higher concentration of chlorides along the whole depth of their drillings. The high quantity of water brought by this poultice seemed to have carried out salts that were distributed more deeply towards more superficial layers. These authors concluded that PDS of the poultice should overlap pore size of the substrate for optimization of desalination efficiency.

Lubelli et al. (2010) analyzed by MIP the same type of poultice that has been applied in this research and determined that the PDS of BW40 cellulose poultice has a sharp peak at 15-20 μm and the BC1000 cellulose poultice shows pores distributed in a slightly wider range between 10 and 30 μm diameter. According to these authors pores of the poultice should be smaller than the pores of the substrate since for desalination the poultice needs to have smaller pores than those of the object for advection to take place (Pel et al. 2010). Water content, grain packing, PDS and pore shape should be also considered in addition to adhesion in order to optimized desalination systems Bourgès and Vergès-Belmin (2008).

The PDS of the analyzed dolostone shows pores distributed in the range between 1 and 3 μm (Fig. 3g), the plaster mortar shows pores in the range 0.1 and 10 μm (Fig. 4f) and the jointing mortar between 1 and 10 μm (Fig. 4e). If the poultice is intended to have the dual purpose of both wetting and desalination, it must have a wide PSD with large pores acting as reservoirs for wetting and small pores to ensure that advection from the substrate towards the poultice takes place, and the object dries before the poultice (Pel et al. 2010). This is the reason because in the analyzed granite, with a polymodal PSD and with most of their pores distributed in the range 100-300 μm (Fig. 3d) could have been more suitable to desalinate with this type of poultice compared to the dolostone or mortar.

Pore structure has a significant influence on salt crystallization, including nucleation and precipitation, capillary rise of solutions, evaporation of water and the effects of the wetting and drying cycles [Benavente et al 2006). As was mentioned above, in order to optimize salt extraction, a poultice working by advection should have smaller pores than the substrate. The porosity present in these cellulose poultices is not small enough to guarantee capillary suction from substrates with pores smaller than 15 μm, i.e. for example no advection will occur when applying these cellulose poultices on the studied dolostone or mortars or even in the smallest pores of the granite sample. This points out how the practice of desalination, mainly relaying on cellulose poultices, is far from being optimized (Lubelli and Van Hess 2010). In our case, it cannot be assured that a higher number of poultice applications could achieve the total reduction of nitrates and sulfates without causing the mobilization of chlorides.

According to Pel et al. (2010) there is no single ideal poulticing method for extracting salts, and that in practice one can never achieve complete desalination of a non moveable object, being therefore more accurate to refer to such interventions as ‘salt content reduction’ rather than ‘desalination’ treatments.

The use of fillers as clays, mixed with cellulose poultice, could be a solution to shift the pore size of the poultice towards smaller pores. Varying the mixtures of bentonite/sand/cellulose a wider range of pores size can be achieved which may be suitable for desalination of substrates with pores larger than 1-2 μm (Lubelli and Van Hess 2010).

In our case study, a higher number of only cellulose poultice applications could increase the efficiency of this desalination procedure. However, since there is no a warrantee of the total extraction of salts, we believe that better preservation strategies are the ventilation system to avoid rising damp and the environmental control.

Determination of the most appropriate environmental conditions

Experimental work: humidity transfer through dolostone

The PDS of dolostone D11 (classified as dolopelmicrite) selected for the experimental work of humidity transfer was characterized at 0.5 cm, 1.5 cm, 3cm and 5 cm from the surface to correlate with the ion chromatography measurements and the relative humidity and temperature data recorded from the environmental control devices (i-buttoms).

The total porosity of the dolostone increases from 24% at 0.5 cm up to 29% at 1.5 cm from the surface (Fig. 9a and Fig. 9b). Total porosity decreases from 29% down to 13% at 1.5 cm and from 13% down to 12% from 3 cm up to 5 cm. PSD curves (Fig.9) show that at all depths the higher amount of pores (56-

94%) are distributed in the range between 1 and 10 µm, specifically, between 1 and 3 µm. Furthermore, there are a significant amount of pores (36-24%) located at depths up to 1.5 cm distributed in the range between 0.1 and 1 µm and a small amount of pores (4-6%) between 0.01 and 0.1 µm. This explains again why the poultice was not able to completely remove the salts from the dolostone. These pores seem that have been generated due to the weathering process by salt crystallization, since at depths of 3 cm (Fig. 9c) most of the pores (94%) are mainly distributed in the range 1-10 µm. At depths of 5 cm from the surface (Fig. 9d) there are a range of pores > 100 µm (13%) that were not present at lower depths.

These results can be correlated with the concentration of soluble salts analyzed at the same depths. From 0.5 cm up to 5 cm from the surface, there is a decrease of sulfate concentration from 33 down to 11 mg/l, a slight increase of nitrates from 5 up to 7 mg/l and an almost constant amount of chlorides of circa 1 g/l. Therefore, sulfates are more concentrated at the surface where there are higher amount of smaller pores < 1 µm, while nitrates are more concentrated deep inside the stone with higher amount of pores > 100 µm. ESEM images and EDX analyses were also carried out at the different depths of this dolostone sample (Fig.9).

Fig.10. Graphs RH transfer

Thermodinamic analyses: salt mixture modelling

Due to the high solubility of epsomite, efflorescences containing this salt are mainly found in places protected from the direct access of rain (Charola and Lewin 1979). The hydration-dehydration of the solid crystals due to environmental conditions variations inside the pores materials causes expansions and contractions breaking of pores giving rise to the disintegration of the building materials (López-Arce et al. 2008). Mg-sulfate induces crack formation and propagation within the bulk stone; epsomite tends to precipitate as anhedral wax-like aggregates formed at high supersaturation and distributed homogeneously throughout the stone pore system, filling large and small pores (Ruiz-Agudo et al. 2007).

The presence of other salts, as chlorides or nitrates modifies the relative humidity in the equilibrium of magnesium sulfate salt (RHeq of epsomite is 90% at 20ºC), lowering down this RHeq. For this reason thermodynamic programs as Runsalt have been carried out in order to know which would be the salt that would precipitate under the different environmental conditions of the cloister. The phase diagram of magnesium sulfate (Fig.11) shows which Mg-sulfate phase would precipitate according to the environmental conditions of Madrid region during winter with average humidity values 75-90% and temperature between 5º and 14ºC (with possibly minimums and maximums between -5ºC and 24ºC). During summer the humidity values range between 54-75% and the temperature range between 14º and 24ºC (with minimums and maximums between 4ºC and 33ºC). The environmental fluctuations can cause the dissolution-crystallization and the hydration-dehydration of magnesium sulfate. For this reason, it is recommendable to control the environmental conditions inside the cloister, to maintain the humidity and temperature constant. According to this phase diagram, and without taking into account the presence of other salts, a suitable range of temperature and humidity to avoid phase transitions, could be in the range 15Cº±5ºC and 60±5%.

Several models of salt crystallization were obtained with the RUNSALT software, changing the environmental conditions to simulate the average temperature of 30ºC during summer and 3ºC during winter. The RH range between 30% and 90% has been considered in both cases.

The results obtained in the mortar sample (DM8) at 0.5 cm depth, during summer (30ºC), before desalination, show that the software mainly predicts the crystallization, of hexahydrite ($MgSO_4 \cdot 6H_2O$) between 70 and 80% RH, starkeyite ($MgSO_4 \cdot 4H_2O$) and niter (KNO_3) between 54 and 70% RH and a slight amount of sylvite (KCl) and halite (NaCl) between 50 and 60%RH (Fig. 12a). The precipitation of these salts is in agreement with our results and with the salts efflorescences collected and analyzed under XRD by López-Acevedo et al. (1996). After desalination, the software mainly predicts the crystallization

of hexahydrite (between 70 and 80% RH), starkeyite (between 50 and 70% RH) and niter (between 42 and 60% RH). However, the amount of precipitation of these salts after desalination is significantly lower than before desalination (Fig. 12b). The prediction model for this sample during winter (3ºC) shows that the main salts that would precipitate before and after desalination would be hexahydrite and niter.

The results obtained in the granite sample (DG1) at 0.5 cm depth, during summer (30ºC), before desalination, show that the software predicts the crystallization, of hexahydrite ($MgSO_4 \cdot 6H_2O$) between 70 and 80% RH and starkeyite ($MgSO_4 \cdot 4H_2O$) between 54 and 70% RH. At lower RH (between 35 and 45%) nitratina ($NaNO_3$) and niter (KNO_3) could also precipitate. Below 40% RH a slight amount of nitromagnesite could precipitate as well (Fig.12c). After desalination, the software predicts the crystallization of niter and halite in a narrow range of RH (between 60 and 63% RH). However, the amount of precipitation of these salts after desalination is almost insignificant and there would be no precipitation of magnesium sulfate, meaning that sulfate reduction has been effective at the surface of the granite stone (Fig.12d). The prediction model for this sample during winter (3ºC) shows the main salt that would precipitate before desalination would be hexahydrite (between 66-90%). Some niter could also precipitate between 50-75%RH. The main salts that would precipitate after desalination would be few amounts of hexahydrite and niter (between 66 and 85%).

Since dolostone is the most common type of stone used in the cloister and the experimental work on humidity transfer was carried out on dolostone samples, the thermodynamic models were applied for this type of stone at different depths.

The results obtained in the dolostone sample (DD7) at different depths and environmental conditions are shown in Table 3. Before desalination, 0.5 cm is the depth at which the software predicts the highest amount and different types of salts at 30ºC. Mainly starkeyite would precipitate between 45-70% RH, hexahydrite between 72-75% RH and sylvite between 48-60% RH. It seems that desalination at this depth has been quite effective, but still some amount of niter and starkeyite would precipitate in the range 42-80% RH. Before desalination, during winter (3ºC), hexahydrite and sylvite would be the salts that would mainly precipitate between 54-88%RH and 50-75% RH, respectively. After desalination, niter would be the main phase precipitated between 50-90%. These results mean that the desalination procedure has not been completely effective, since after desalination, in spite of there would precipitate lesser amount and lesser types of salts still nitrates and magnesium sulfates would precipitate at higher and a broader range of RH. At higher depths (1-3cm) there are less precipitation of salts, although it seems that after desalination and specially at lower temperatures (3ºC) there are more quantity of salts also at higher and a broader range of RH. At 5 cm depth, the software predicts the precipitation of similar types and amounts of salts before and after desalination in both summer and winter seasons meaning once again that the desalination procedure has not been effective in the dolostone.

Since Mg-sulfate (epsomite) is the most abundant salt present in the building materials from the cloister, to avoid its phase transition the most suitable conditions, according to the Mg-sulfate phase diagram, these were established at temperature 15ºC±5 and 60%±5 RH. In order to predict the most suitable conditions to avoid salt crystallization, the ion chromatography values obtained in the dolostone (D2D7) at different depths after desalination were introduced in Runsalt software at temperatures above and below 15ºC and a range of RH between 35-65% (Table 4).

At 20ºC, the software predicts the crystallization of starkeyite, niter, sylvite and halite in a RH range between 53 and 65% at depths up to 1 cm. At higher depths the software predicts mainly the precipitation of nitromagnesite, niter and nitratine in a RH range circa 35-45%.

At 15ºC, the software predicts the crystallization of hexahydrite, niter and sylvite in a RH range between 62 and 65% at depths of 0.5 and 1 cm. At higher depths the software predicts mainly the precipitation of nitromagnesite, niter and nitratine in a RH range circa 35-48%.

At 10ºC, the software predicts the crystallization of halite in a RH range 53-60% at 0.5 cm, and hexahidrite, niter and sylvite in a narrow RH range between 64 and 65% at 1 cm. At higher depths the software predicts mainly the precipitation of nitratine, nitromagnesite and starkeyite in a RH range circa 35-50%.

According to these results, the environmental conditions to avoid salt crystallization at the three selected temperatures would be 20ºC and 50±5% RH or 15ºC and 55±5% or 10ºC and 51-52% RH. Since 20ºC and 50±5% RH is critical point located between the boundaries of phase transition hexahydrite-epsomite (Fig.11) and any slight fluctuation above and below these values can cause the hydration or dehydration of these phases, this condition is rejected for environmental control. By other hand, 10ºC and 51-52% RH conditions is in a narrow range of RH, since below and above 51-52% precipitation of salts can occur. Furthermore, 10ºC is considered a very cold temperature to keep in the cloister. Therefore, 17º±2ºC and 55±2% RH could be considered as suitable conditions to avoid salt crystallization in the cloister close to the most suitable environmental conditions of 15ºC and 55±5%.

Conclusion

In order to solve the salt crystallization process (mainly Mg-sulfates) and the consequent deterioration of building materials and to keep the stability of some significant paintings that will be exposed inside the cloister from El Paular Monastery, after a first diagnostic or characterization of building materials and salts, we have established three preservation strategies based on architectural, pethophysical and physical-chemical features:

1- The main source of Mg-sulfate salts seems to be the high concentration of moisture and the raising damp by capillarity, especially through the mortars which are the most porous materials. The dissolution of gypsum (calcium sulfate) as component of the mortars and the interaction with magnesium also from the mortars, granite and dolostone can easily precipitate Mg-sulfates that migrate through the porous building materials. Since the are also presence of other salts, as chlorides or nitrates, thermodynamic models have been carried with Runsalt software in order to know which would be the salts that would precipitate under the different environmental conditions of the cloister and which would be the most suitable conditions.

2- The installation of a ventilation system would avoid the rising damp and hence the dissolution, mobilization and crystallization of salts.

3- The salt reduction of building materials have been performed with cellulose poultices with pores between 15-20 μm and between 10 and 30 μm diameter. The PDS of the analyzed dolostone shows a monomodal distribution of pores distributed in the range between 1 and 3 μm, the plaster mortar shows pores in the range 0.1 and 10 μm and the jointing mortar between 1 and 10 μm. The analyzed granite, with a polymodal PSD and with most of their pores distributed in the range 100-300 μm has been the most effective material to desalinate with this type of poultice. A higher number of cellulose poultice applications could increase the efficiency of this desalination procedure. However, there is no a warrantee of the total extraction of salts and the mixture of this cellulose poultice with clays to shift the PSD to smaller sizes would be more efficient to desalinate dolostone or mortar.

4- The determination of the most suitable environmental conditions, inferred from thermodynamic model predictions and experimental work based on relative humidity transfer inside the stone, to avoid salt crystallization would be 20ºC and 50±5% RH or 15ºC and 55±5% or 10ºC and 51-52% RH. Since 20ºC and 50±5% RH is a critical point located between the boundaries of phase transition hexahydrite-epsomite; 10ºC and 51-52% RH conditions is in a narrow range of RH and 10ºC is considered a very cold temperature to keep in the cloister, the most suitable environmental conditions could be 17º±2ºC and 55±2% RH.

However, if the ventilation system or the environmental control fails for some reasons, there would be a risk of precipitation and mobilization of the remaining salts after poulticing since it has not been totally effective. Therefore, we would recommend keeping the paintings that will be exposed on the walls of the cloister inside glass cases.

Acknowledgments

This study was funded by GEOMATERIALES (S2009/MAT-1629) and CONSOLIDERTCP (CSD2007-0058). Thanks to the UCM Research Group "Alteración y Conservación de los Materiales Pétreos del Patrimonio" (ref. 921349). We are grateful to Eduardo Barceló de Torres for some plans and drafts of the monastery. Thanks also to SOPSA, S.A company for his help and collaboration during the sampling collection and restoration works. The authors thank the JAE-Doc CSIC contract for supporting P.López-Arce to develop this work. The authors are also grateful to Laura Tormo and Marta Furió of the Natural Science Museum (CSIC) for providing the ESEM-EDS photographs and analyses. Special thanks go to Inmaculada Ruiz, Iván Serrano, Javier Rodriguez, David Freire and Luz Gómez-Villalba, IGE (Institute of Economic Geology) petrophysics laboratory technicians.

References

AENOR Spanish Association for Standardisation and Certification UNE-EN 1936:1999. Natural stone test methods. Determination of real density and apparent density, and of total and open porosity.

AENOR Spanish Association for Standardisation and Certification UNE-EN 14579:2005. Natural stone test methods. Determination of sound speed propagation.

AENOR Spanish Association for Standardisation and Certification UNE-EN 13755:2002. Natural stone test methods. Determination of water absorption at atmospheric pressure.

AENOR Spanish Association for Standardisation and Certification UNE-EN 1925:1999. Natural stone test methods. Determination of water absorption coefficient by capillarity.

Benavente D, Garcia del Cura MA, Ordoñez S (2003) Salt influence on evaporation from porous building rocks. Construction and building Materials 17(2):113-122.

Benavente D, Garcı´a del Cura MA, Fort R, Ordoñez S (2004) Durability estimation of porous building stonesfrom pore structure and strength. Eng Geol 74(1–2):113–127

Benavente D, Linares-Fernandez L, Cultrone G, Sebastian E (2006) Influence of microstructure on the resistance to salt crystallisation damage in brick. Mater Struct 39(1):95–101

Benavente D, Cueto N, Martinez-Martinez J, Garcia del Cura MA, Cañaveras JC (2007) The influence of petrophysical properties on the salt weathering of porousbuilding rocks. Environ Geol 39:105–113

Bourgès and Vergès-Belmin (2008). Comparison and optimization of five desalination systems on the inner walls of Saint Philibert Church in Dijon, France. In: Proceedings from the International Conference on Salt Weathering on Building and Stone Sculptures. 22-24 October 2008, The National Museum Copenhagen, Denmark. P.29-40.

Bruni S, Cariati F, Fermo P, Pozzi A, Toniolo L (1998). Characterization of ancient magnesian mortars coming from Northern Italy. Thermochim Acta 321:161–5.

Caner EN, Demirci SA, Turkmenoglu G (1985). Deterioration of dolomite by soluble salts in Divrigi Mosque-Turkey". 5th Int. Cong. On Deterioration and Conservation of Stone, Lausanne, 299-305.

Charola AE, Lewin SZ (1979). Efflorescences on building stones – SEM in thecharacterization and elucidation of mechanisms of formation. Scan Electron Microsc 1:379–86.

Chiari G, Santarelli ML, Torraca G (1992). Caratterizzazione delle malte antiche mediante lánalisi di campioni non fracio. Materiali e strutture: Problema di conservazione II(3):111–37.

Cooke RU, Gibbs GB (1991). Crumbling Heritage? Studies of stone weathering in polluted atmospheres. National Power PLC and PowerGen plc.

David Young (2008). Salt attack and rising damp: A guide to salt damp in historic and older buildings. Technical report: Heritage Council of NSW. Heritage Victoria, South Australian Department for Environment and Heritage Adelaide City Council. 78 pp.

Fernández-Díaz L, Pina CM, Astilleros JM and Sánchez-Pastor N (2009). The carbonation of gypsum: Pathways and pseudomorph formation. American Mineralogist 94: 1223-1234.

Fort R, Fernández-Revuelta B, Varas MJ, Álvarez de Buergo M, Taborda M (2008). Effect of anisotropy on Madrid-region Cretaceous dolostone durability in salt crystallization processes Mater Construcc 58(289-290):161-177.

Gómez-Heras M, Benavente D, Alvarez De Buergo M and Fort R (2004). Soluble salt minerals from pigeon droppings as potential contributors to the decay of stone based Cultural Heritage. Eur J Mineral 16:505-509.

Gonzalez Limon T, Alvarez de Buergo Ballester M (2002). Los revocos de cal de las fachadas de la plaza de la Corredera de Cordoba – the lime renderings from plaza de la Corredera. Cordoba Mater Construcc 52(267):19–30.

Klemm W, Siedel H (1996). Sources of sulphate salt efflorescences at historical monuments – a geochemical study from Freiberg, Saxony. In: Riederer J, editor. Proceedings of the eighth international congress on deterioration and conservation of stone, vol. 1. Berlin, Germany. p. 489–95.

Laurie AP (1925). Stone decay and the preservation of buildings. J Soc Chem Ind;27:86–92.

La Iglesia A, Garcia del Cura MA and Ordoñez S (1994). The physicochemical weathering of monumental dolostones, granites and limestones; dimension stones of the Cathedral of Toledo (Spain). Sci Total Environ 152:179–88.

López-Acevedo MV, Algaba M, García E, Martín-Vivaldi JL and Soutullo B. (1996): Estudio de las alteraciones en el claustro principal del Monasterio de El Paular, Madrid. 23 pp. Proyecto H061/91 Plan Regional de Humanidades y Ciencias Sociales de la Comunidad de Madrid.

Lopez-Arce P, Doehne E, Martin W, Pinchin S (2008) Magnesium sulfate salts and historic building materials: experimental simulation of limestone flaking by relative humidity cycling and crystallization ofsalts]. Mater Construcc 58(289–290):125–142 .

López-Arce P, Garcia-Guinea J, Benavente D, Tormo L, Doehne E (2009a). Deterioration of dolostone by magnesium sulphate salt: an example of incompatible building materials at Bonaval Monastery, Spain. Constr Build Mater 23(2):846–55.

López-Arce P, Doehne E, Greenshields J, Benavente D. and Young D. (2009b). 'Treatment of rising damp and salt decay: the historic masonry buildings of Adelaide, South Australia'. Materials and Structures 42:827–848.

López-Arce P, Varas-Muriel MJ, Fernández-Revuelta B, Alvárez de Buergo M, Fort R. and Pérez-Soba C. (2010) Durability of Spanish granites exposed to salt crystallization tests: surface roughness quantification. Catena (in press).

Lubelli B and van Hees RPJ (2010). Desalination of masonry structures: Fine tuning of pore size distribution of poultices to substrate properties J Cult Heritage 11:10-18.

Pel L, Sawdy A and Voronina V (2010). Physical principles and efficiency of salt extraction by poulticing J Cult Heritage 11:10-18.

Pitzer KS (1973) J Phys Chem 77: 268-277.

Price CA (2000) An expert chemical model for determining the environmental conditions needed to prevent salt damage in porous materials. European Commision. Protection and Conservation of European Cultural Heritage. Research Report 11. Archetype, London.

Schaffer RJ (1932). The weathering of natural building stones. London: HMSO, Department of Scientific and Industrial Research Special Report.

Ruiz-Agudo E, Mees F, Jacobs P, Rodriguez-Navarro C (2007). The role of saline solution properties on porous limestone salt weathering by magnesium and sodium sulfates. Environ. Geol, 52(2):269-281.

Tulliani JM, Bertollini Cestari C (2005). Study of the degradation causes affecting stucco sculptures from the Valentino Castle in Turín. Mater Struct 38:425–32.

Viles HA and Goudie AS (2007). Rapid salt weathering in the coastal Namib desert: Implications for landscape development. Geomorphology 85:49-62.

Villaseñor I and Price CA (2008) Technology and decay of magnesian lime plasters: the sculptures of the funerary crypt of Palenque, Mexico. J Archaeol Sci 35:1030-1039.

Villegas Sanchez R, Martin Garcia L, Vale Parapar JF, Bello Lopez MA, Alcalde Moreno M (1996). Characterization and conservation of the stone used in the cathedral of Almeria (Spain). In: Riederer J, editor. Proceedings of the eighth international congress on deterioration and conservation of stone, vol. 1. Berlin, Germany. p. 89–99.

FIGURE CAPTIONS

Figure 1 Map of the cloister from El Paular monastery and areas of sampling

Figure 2 Location of salt efflorescences and drillings of building materials performed in the NE corner of the cloister. Relative humidity and temperature values were also measured inside the drillings DG2, DM4, DD7, DM8, DD15 and DM16

Figure 3 Characterization of stone building materials from El Paular monastery: a) Polarized light optical microscopy image (PLOM) of inner area of granite sample G7 from the basement; b) PLOM image of outer area of granite sample G1 from the pavement ; c) Pore size distribution (PSD) of inner area of granite sample G1; d) PSD of outer area of granite sample G1; e) PLOM image of dolostone sample D1; f) PLOM image of dolostone sample D2 (dolobiomicrite); g) PSD of dolostone sample D1 (dolopelmicrite); h) PSD of dolostone sample D2

Figure 4 ESEM and XRD characterization of mortars from El Paular monastery: a) ESEM image of plaster mortar sample MP17; b) XRD pattern of the external and inner layer of plaster mortar sample MP17; c) ESEM image of jointing mortar sample MJ7; d) XRD pattern of jointing mortar sample MJ7; e) PSD of jointing mortar sample MJ10; f) PSD of plaster mortar sample MP17

Figure 5 ESEM-EDS analyses maps of jointing mortar sample (MJ10). a) ESEM image; b) Magnesium mapping (Mg) in red color; c) Sulfur mapping (S) in yellow color; d) Calcium mapping (Ca) in blue color; e) Chloride mapping (Cl) in pink color; f) Sodium mapping (Na) in green color

Figure 6 Soluble salts distribution maps displaying the amount of sulfates, nitrates and chlorides with depth and height of the different building materials along the drilled wall: a) distribution map of sulfates in stone and brick samples; b) distribution map of sulfates in mortar samples; c) distribution map of nitrates in stone and brick samples; d) distribution map of nitrates in mortar samples; e) distribution map of chlorides in stone and brick samples; f) distribution map of chlorides in mortar samples

Figure 7 XRD and ESEM analyses of salt efflorescences from the cloister. a) XRD pattern; b) ESEM image

Figure 8 Bar diagrams displaying the amount of anions (sulfates, nitrates and chlorides) with depth (from 0.5 cm up to 5 cm) on the different building materials (granite, dolostone and mortar) analyzed with ion chromatography before and after desalination

Figure 9 Pore size distribution by mercury intrusion porosimetry, Ion Chromatography results and ESEM images at 0.5 cm, 1.5cm, 3cm and 5 cm from the surface of the dolostone (D11) selected for experimental work on humidity transfer

Figure 10 Graphs showing relative humidity (RH) transfer through dolostone samples

Figure 11 Phase diagram showing relative humidity vs. temperature for $MgSO_4$–H_2O system. The environmental conditions in summer and winter for the region of Madrid and the suitable range of RH and temperature to avoid phase transition inside the cloister are shown

Figure 12 Crystallization sequence of the soluble salts as a function of RH calculated with RUNSALT software: a) Mortar sample (DM8) at 0.5 cm depth before desalination; b) Same sample after desalination; c) Granite sample (DG1) at 0.5 cm depth before desalination; d) Same sample after desalination

Table 1 X-Ray diffraction of mortar samples (MP, plaster mortar; MJ, jointing mortar) from the cloister

Location	Mortar	Binder			Aggragates					Salts
		Calcite	Dolomite	Gypsum	Quartz	Feldspar (K)	Plag.	Biotite	Clays	Epsomite
West Hallway	MJ1-MJ2	x			x					
	MJ3	x		x	x	x	x	x		x
	MP4	x			x					x
	MP5	x			x					x
	MJ6	x	x		x		x		x	x
	MP7	x	x	x	x			x		x
	MJ8	x		x	x	x		x		
	MJ18	x		x	x					
North Hallway	MJ9	x	x	x	x					
	MJ10	x			x					
	MP16	x		x						
	MP17	x		x	x					
		x			x	x	x	x		x
		x	x		x	x	x	x		x
	MJ19	x	x		x	x				x
	MJ20	x	x		x					x
	MP21	x	x	x	x					
	MJ24	x		x	x	x	x	x		x
East Hallway	MJ11	x		x	x	x		x		
	MJ12	x		x	x	x	x	x		
	MJ13	x			x	x	x			
	MJ14	x		x	x	x	x	x		
	MJ15	x	x	x	x	x	x	x	x	
	MJ22	x	x		x	x				x
	MJ23	x		x	x					x
	MJ25	x			x					

Table 2 Salt concentration, anions (mg/l) and conductivity (μS/cm) in cellulose poultices

Application	Poultice sample	Material	Conductivity	Sulphates	Nitrates	Nitrites	Chlorides	Fluorides
1	PAP.G1	Granite (DG1)	256	52.8	9.5	0.33	7.88	0.13
2	PAP.G2		257	63.07	3.18	0.42	5.08	0.24
3	PAP.G3		155	29.7	1.82	0.08	1.93	0.14
4	PAP.G4		88	8.51	0.21	0	0.9	0.11
5	PAP.G5		79	6.05	0.54	0	1.55	0.08
1	PAP.M1	Mortar (DM8)	90	2.01	0.81	0.12	1.23	0.41
2	PAP.M2		57	1.1	0.62	0.07	0.79	0.2
3	PAP.M3		58	0.86	0.4	0.27	0.47	0.1
4	PAP.M4		41	1.73	0.37	0.23	0.62	0.1
5	PAP.M5		41	1.02	0.46	0.25	1.39	0.14
1	PAP.D1	Dolostone (DD7)	80	1.95	0.82	0.1	0.72	0.07
2	PAP.D2		62	0.5	0.62	0.55	0.47	0.2
3	PAP.D3		54	0.82	0.32	0.25	0.54	0.11
4	PAP.D4		50	1.41	0.28	0.29	0.55	0.07
5	PAP.D5		37	0.9	0.39	0.25	1.12	0.21

Table 3 Salt crystallization predictions on dolostone sample DD7 at different depths at 30ºC and 3ºC, using ion chromatography data and Runsalt software

Depth (cm)	Summer (30ºC)				Winter (3ºC)			
	Before desalination	RH (%) range	After desalination	RH (%) range	Before desalination	RH (%) range	After desalination	RH (%) range
0.5	Hexahydrate Starkeyite Sylvite Halite Carnallite	72-78 45-70 48-60 50-54 35-45	Niter Starkeyite	42-80 42-60	Hexahydrate Sylvite Halite Carnallite	54-88 50-70 52-56 45-50	Niter Hexahydrate	50-90 50-75
1	Halite Carnallite	30-38 30-32	Niter Sylvite Starkeyite Halite	42-74 44-70 44-64 44-56	Nitromagnesite Carnallite Halite	30-38 30-39 30-40	Niter Sylvite Hexahydrate Halite	50-90 52-76 52-75 52-60
1.5	Nitromagnesite	30-34	No precipitation	N/a	Nitromagnesite Carnallite	30-44 30-35	Carnallite Halite Nitromagnesite	30-38 30-36 30-38
3	No precipitation	N/a	Starkeyite	35-67	Nitromagnesite Carnallite Halite	30-41 30-36 30-34	Hexahydrate Nitromagnesite Starkeyite	45-79 45-52 35-44
5	Hexahydrate Starkeyite Nitromagnesite	70-80 56-68 35-44	Starkeyite	35-70	Hexahydrate Nitromagnesite	70-90 45-54	Hexahydrate Niter	66-82 54-66

Table 4 Salt crystallization predictions on dolostone sample DD7 after desalination at different depths under the suitable predicted environmental conditions (temperature 20ºC, 15ºC and 10ºC)

Depth (cm)	(20ºC; 35-65% RH)	RH (%) range	(15ºC; 35-65% RH)	RH (%) range	(10ºC; 35-65% RH)	RH (%) range
0.5	Halite	53-59	Hexahydrite	63-65	Halite	53-60
	Starkeyite	56-63	Niter	63-65		
	Sylvite	56-63	sylvite	63-65		
1	Starkeyite	60-62	Hexahydrite	62-65	Hexahydrite	64-65
	Sylvite	60-62	Niter	62-65	Niter	
	Niter	60-65	sylvite	62-63	sylvite	
1.5	Nitratine	35-41	Nitratine	36-43	Nitratine	36-45
	Niter	35-47	Nitromagnesite	35-49	Nitromagnesite	36-50
	Nitromagnesite	35-47	Niter	41-48	Starkeyite	42-50
	Starkeyite	55-63				
3	Niter	35-42	Nitratine	35-44	Nitromagnesite	35-46
	Nitromagnesite	35-42	Nitromagnesite	35-44	Nitratine	36-46
	Nitratine	35-42	Niter	35-44	Starkeyite	41-45
	Starkeyite	53-63				
5	Nitromagnesite	35-45	Nitromagnesite	35-47	Nitromagnesite	35-48
	Nitratine	35-43	Nitratine	36-45	Nitratine	36-47
	Niter	41-45				

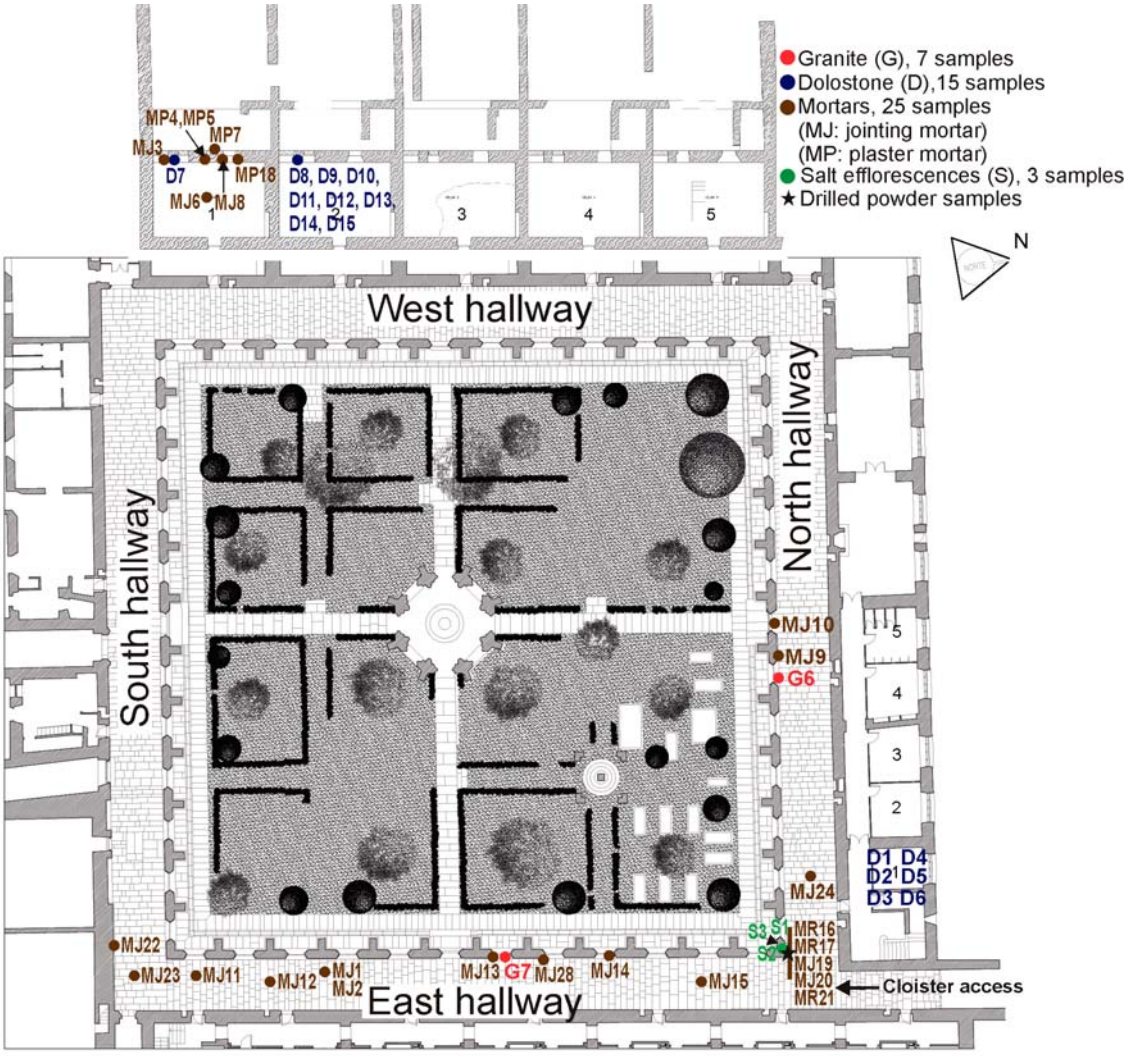
Granite (G), 7 samples
Dolostone (D),15 samples
Mortars, 25 samples
(MJ: jointing mortar)
(MP: plaster mortar)
Salt efflorescences (S), 3 samples
Drilled powder samples
MP4,MP5
MP7
MJ3
D7
MP18
MJ6
MJ8
D8, D9, D10,
D11, D12, D13,
D14, D15
1
2
3
4
5
N
West hallway
South hallway
North hallway
East hallway
MJ10
MJ9
G6
D1 D4
D2 D5
D3 D6
MJ24
S3 S1
S2
MR16
MR17
MJ19
MJ20
MR21
Cloister access
MJ22
MJ23
MJ11
MJ12
MJ1
MJ2
MJ13
G7
MJ28
MJ14
MJ15

FIGURE 1

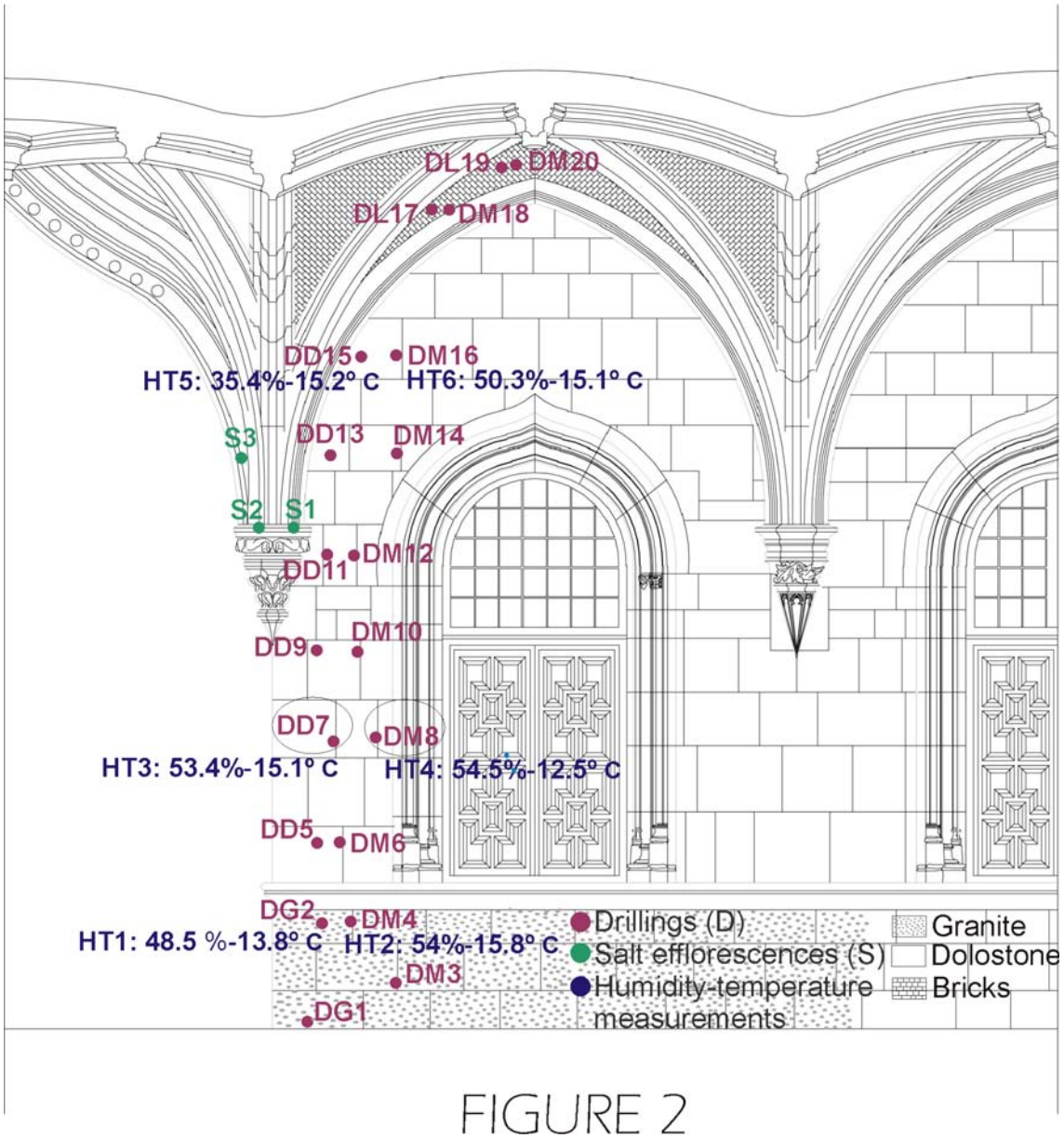
DL19
DM20
DL17
DM18
DD15
DM16
HT5: 35.4%-15.2º C
HT6: 50.3%-15.1º C
S3
DD13
DM14
S2
S1
DM12
DD11
DM10
DD9
DD7
DM8
HT3: 53.4%-15.1º C
HT4: 54.5%-12.5º C
DD5
DM6
DG2
DM4
HT1: 48.5 %-13.8º C
HT2: 54%-15.8º C
DM3
DG1
Drillings (D)
Salt efflorescences (S)
Humidity-temperature measurements
Granite
Dolostone
Bricks

FIGURE 2

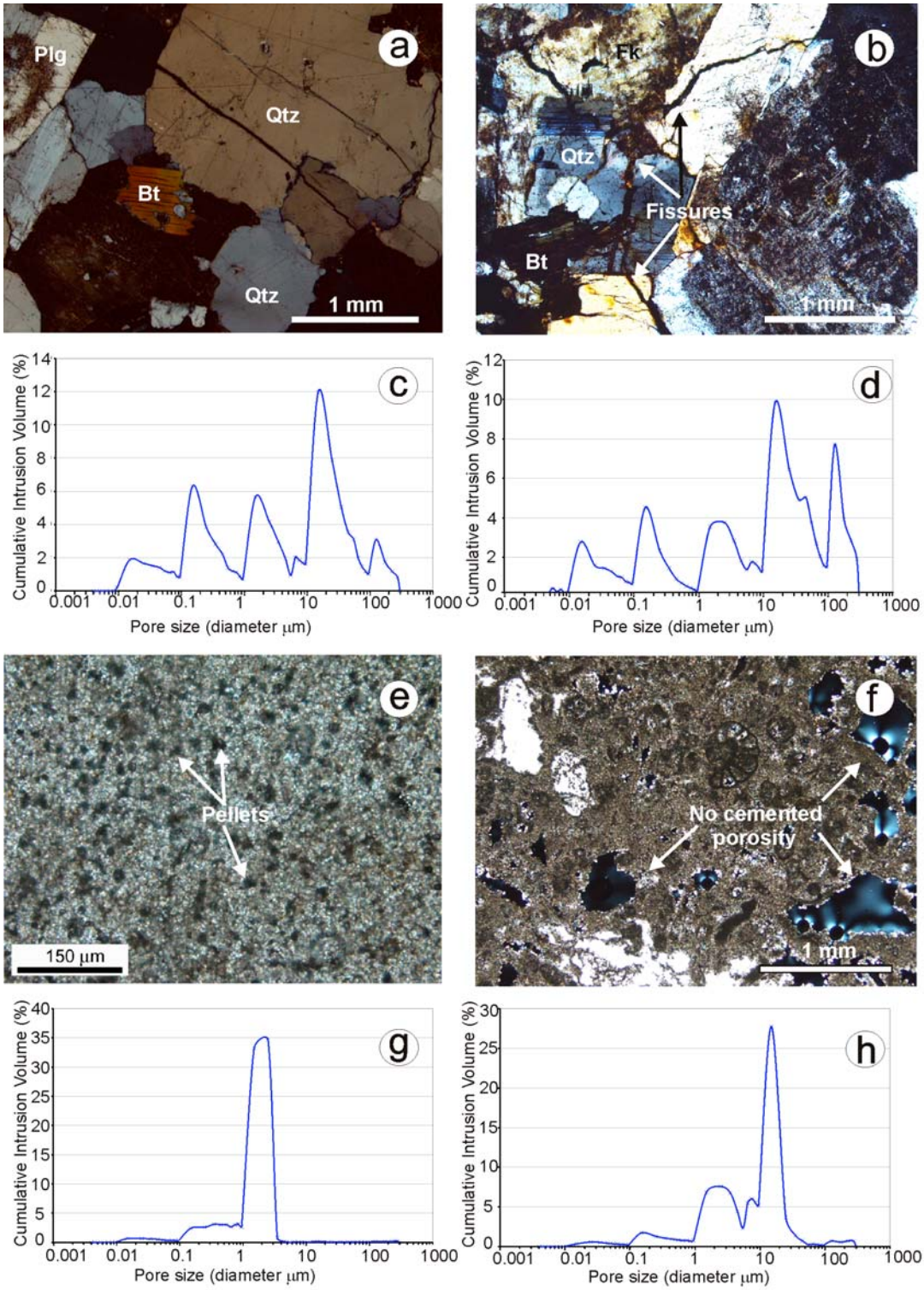
a
Plg
Qtz
Bt
Qtz
1 mm
b
Fk
Qtz
Fissures
Bt
1 mm
c
Cumulative Intrusion Volume (%)
Pore size (diameter μm)
d
Cumulative Intrusion Volume (%)
Pore size (diameter μm)
e
Pellets
150 μm
f
No cemented porosity
1 mm
g
Cumulative Intrusion Volume (%)
Pore size (diameter μm)
h
Cumulative Intrusion Volume (%)
Pore size (diameter μm)

FIGURE 3

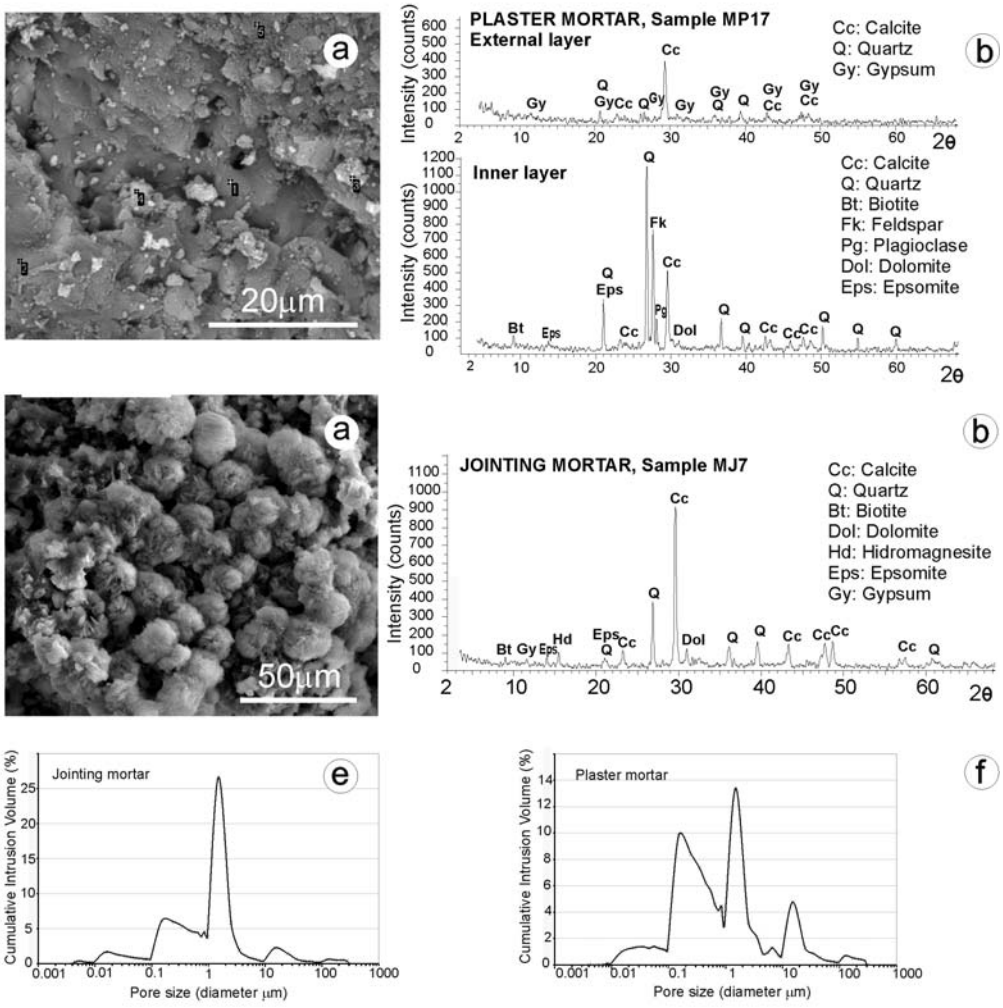
a
20μm
PLASTER MORTAR, Sample MP17
External layer
Cc: Calcite
Q: Quartz
Gy: Gypsum
b
Intensity (counts)
2θ
Inner layer
Cc: Calcite
Q: Quartz
Bt: Biotite
Fk: Feldspar
Pg: Plagioclase
Dol: Dolomite
Eps: Epsomite
a
50μm
b
JOINTING MORTAR, Sample MJ7
Cc: Calcite
Q: Quartz
Bt: Biotite
Dol: Dolomite
Hd: Hidromagnesite
Eps: Epsomite
Gy: Gypsum
Jointing mortar
e
Cumulative Intrusion Volume (%)
Pore size (diameter μm)
Plaster mortar
f

FIGURE 4

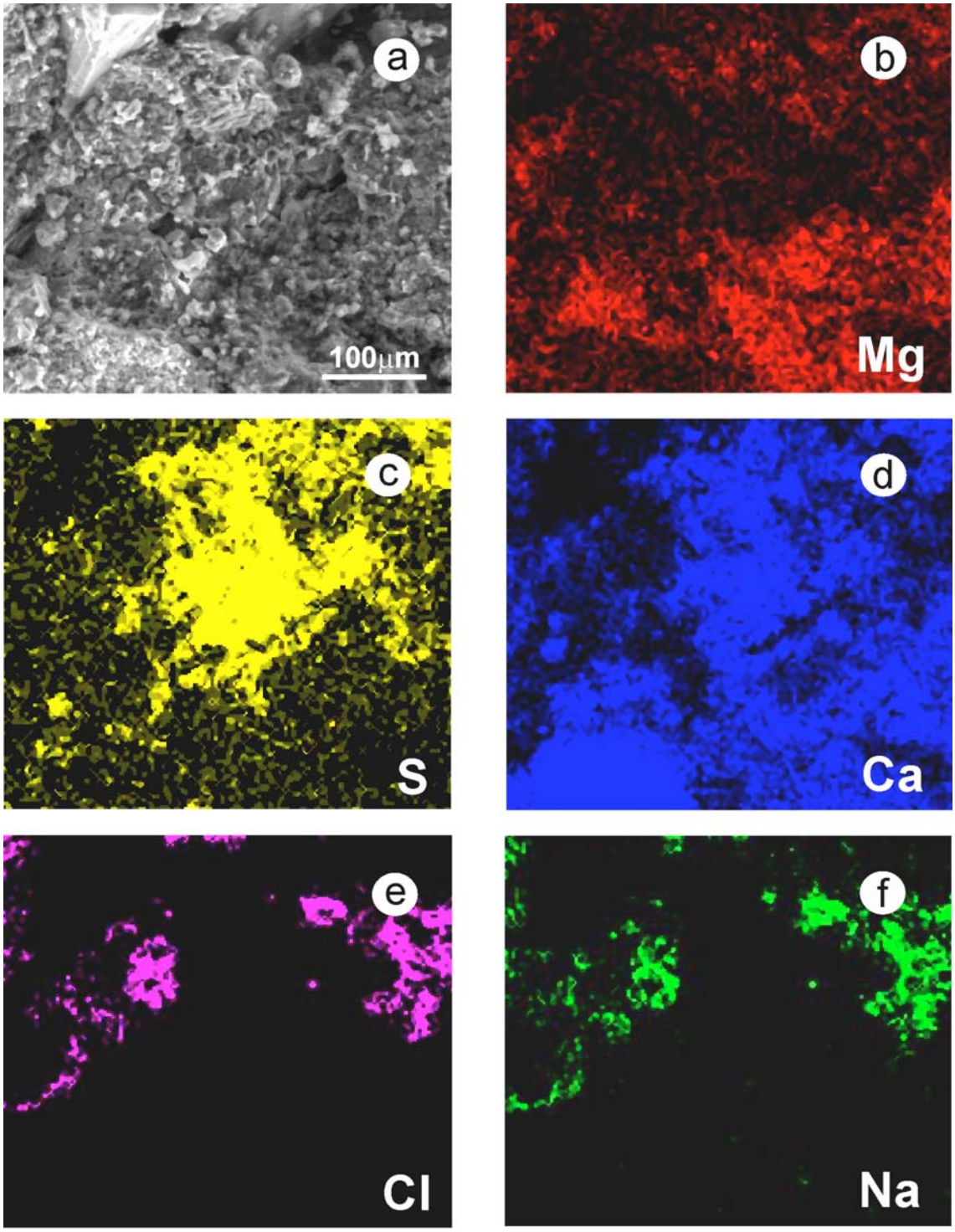

FIGURE 5

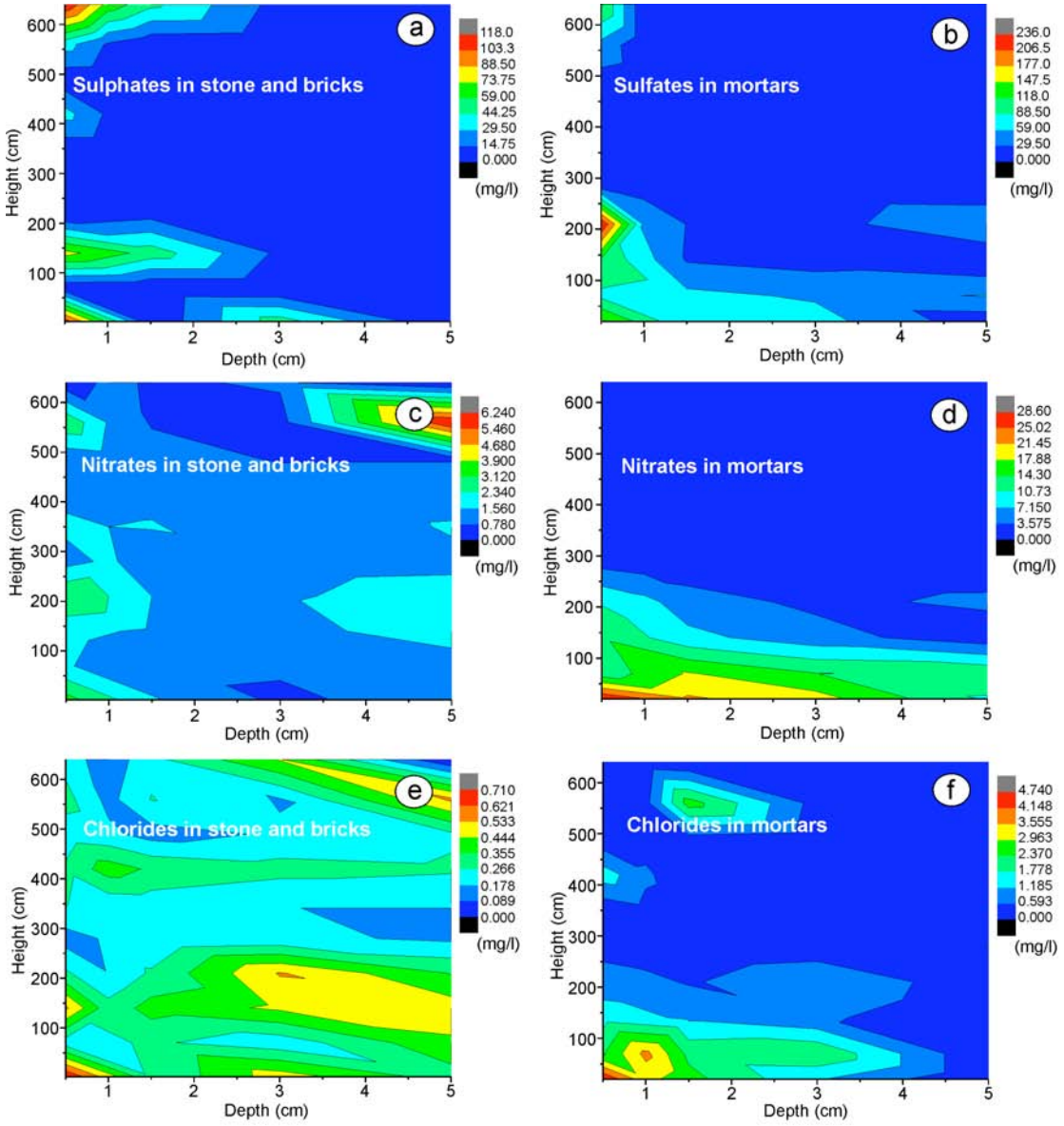
a
Sulphates in stone and bricks
118.0
103.3
88.50
73.75
59.00
44.25
29.50
14.75
0.000
(mg/l)
b
Sulfates in mortars
236.0
206.5
177.0
147.5
118.0
88.50
59.00
29.50
0.000
(mg/l)
c
Nitrates in stone and bricks
6.240
5.460
4.680
3.900
3.120
2.340
1.560
0.780
0.000
(mg/l)
d
Nitrates in mortars
28.60
25.02
21.45
17.88
14.30
10.73
7.150
3.575
0.000
(mg/l)
e
Chlorides in stone and bricks
0.710
0.621
0.533
0.444
0.355
0.266
0.178
0.089
0.000
(mg/l)
f
Chlorides in mortars
4.740
4.148
3.555
2.963
2.370
1.778
1.185
0.593
0.000
(mg/l)
Height (cm)
Depth (cm)

FIGURE 6

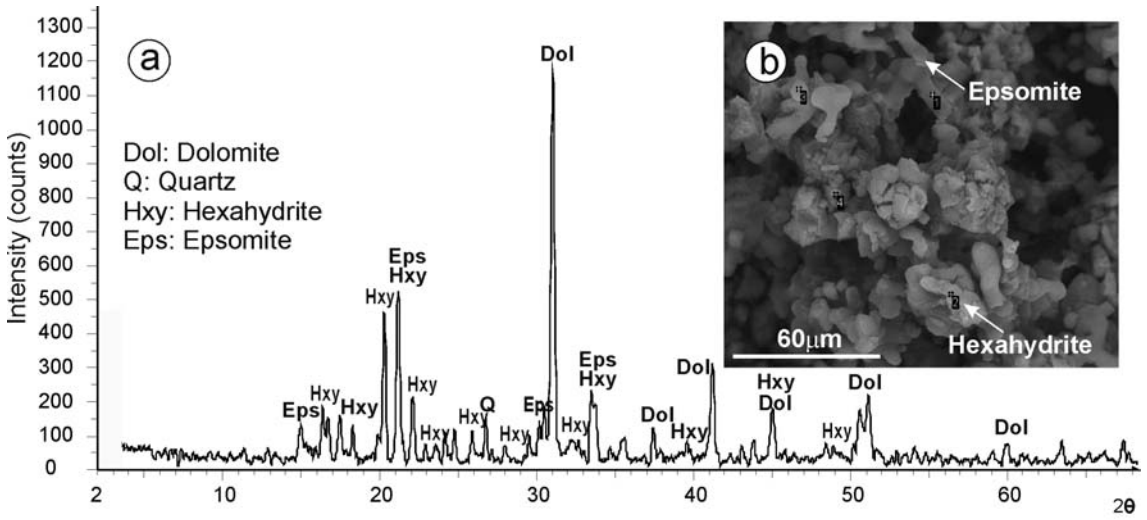
a
Dol: Dolomite
Q: Quartz
Hxy: Hexahydrite
Eps: Epsomite
Intensity (counts)
2θ
b
Epsomite
Hexahydrite
60μm

FIGURE 7

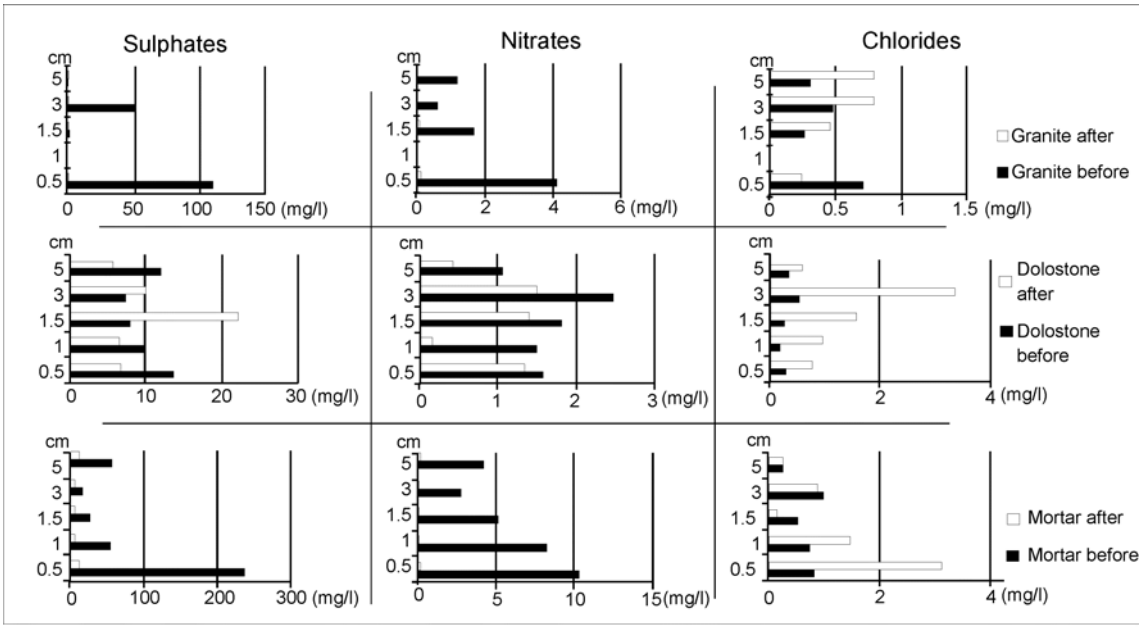
Sulphates
Nitrates
Chlorides
cm
5
3
1.5
1
0.5
0 50 100 150 (mg/l)
0 2 4 6 (mg/l)
0 0.5 1 1.5 (mg/l)
Granite after
Granite before
0 10 20 30 (mg/l)
0 1 2 3 (mg/l)
0 2 4 (mg/l)
Dolostone after
Dolostone before
0 100 200 300 (mg/l)
0 5 10 15(mg/l)
0 2 4 (mg/l)
Mortar after
Mortar before

FIGURE 8

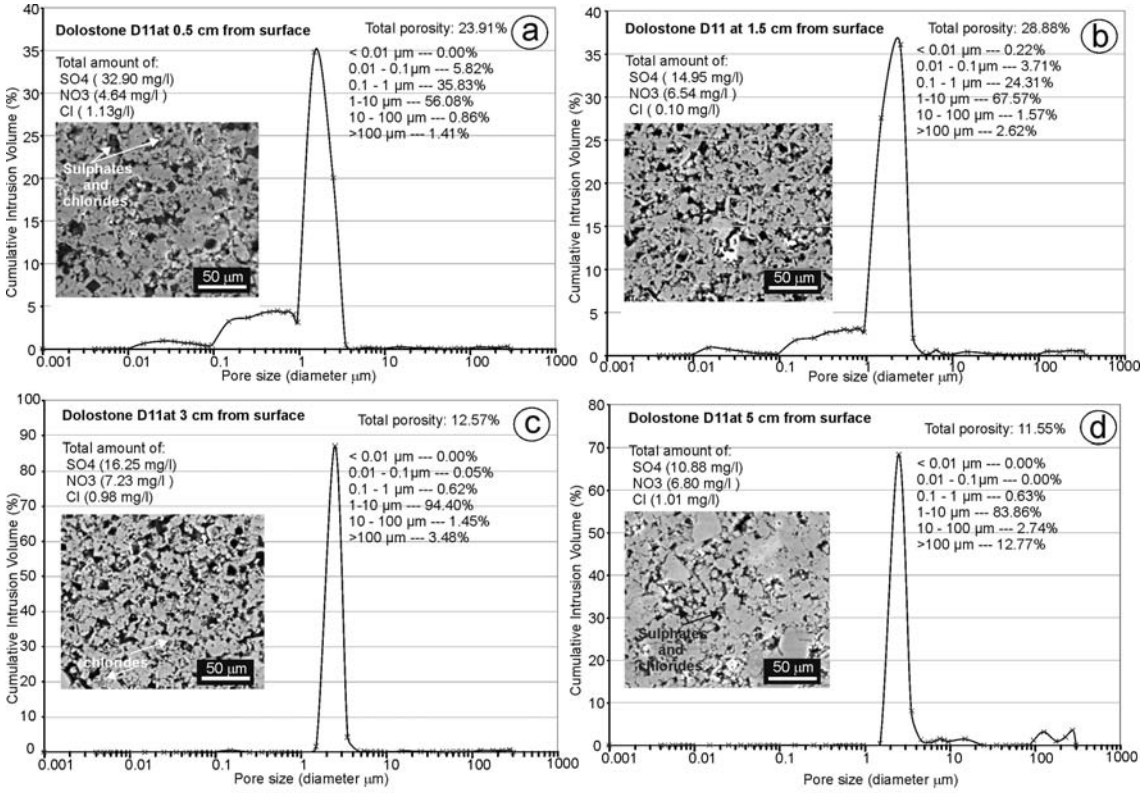
Dolostone D11at 0.5 cm from surface
Total porosity: 23.91%
a
Total amount of:
SO4 (32.90 mg/l)
NO3 (4.64 mg/l)
Cl (1.13g/l)
< 0.01 µm --- 0.00%
0.01 - 0.1µm --- 5.82%
0.1 - 1 µm --- 35.83%
1-10 µm --- 56.08%
10 - 100 µm --- 0.86%
>100 µm --- 1.41%
Sulphates and chlorides
50 µm
Dolostone D11 at 1.5 cm from surface
Total porosity: 28.88%
b
Total amount of:
SO4 (14.95 mg/l)
NO3 (6.54 mg/l)
Cl (0.10 mg/l)
< 0.01 µm --- 0.22%
0.01 - 0.1µm --- 3.71%
0.1 - 1 µm --- 24.31%
1-10 µm --- 67.57%
10 - 100 µm --- 1.57%
>100 µm --- 2.62%
50 µm
Dolostone D11at 3 cm from surface
Total porosity: 12.57%
c
Total amount of:
SO4 (16.25 mg/l)
NO3 (7.23 mg/l)
Cl (0.98 mg/l)
< 0.01 µm --- 0.00%
0.01 - 0.1µm --- 0.05%
0.1 - 1 µm --- 0.62%
1-10 µm --- 94.40%
10 - 100 µm --- 1.45%
>100 µm --- 3.48%
Chlorides
50 µm
Dolostone D11at 5 cm from surface
Total porosity: 11.55%
d
Total amount of:
SO4 (10.88 mg/l)
NO3 (6.80 mg/l)
Cl (1.01 mg/l)
< 0.01 µm --- 0.00%
0.01 - 0.1µm --- 0.00%
0.1 - 1 µm --- 0.63%
1-10 µm --- 83.86%
10 - 100 µm --- 2.74%
>100 µm --- 12.77%
Sulphates and chlorides
50 µm
Cumulative Intrusion Volume (%)
Pore size (diameter µm)

FIGURE 9

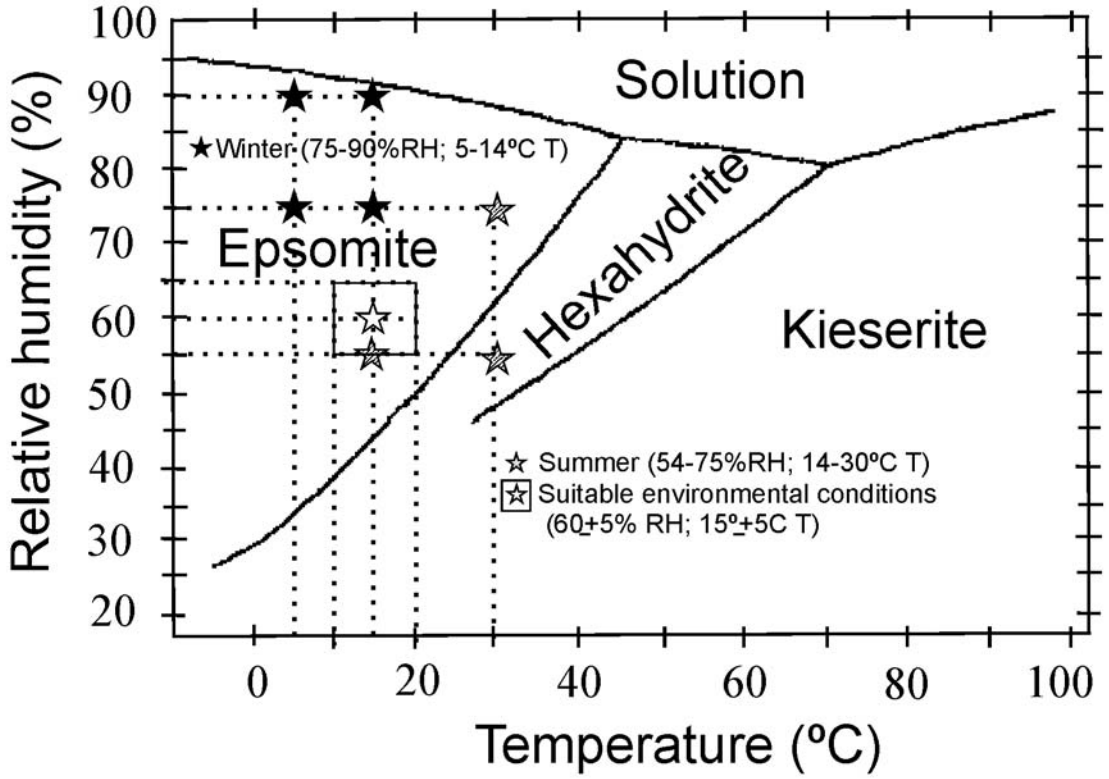
Relative humidity (%)
100
90
80
70
60
50
40
30
20
0
20
40
60
80
100
Temperature (ºC)
Solution
Winter (75-90%RH; 5-14ºC T)
Epsomite
Hexahydrite
Kieserite
Summer (54-75%RH; 14-30ºC T)
Suitable environmental conditions
(60±5% RH; 15º±5C T)

FIGURE 11

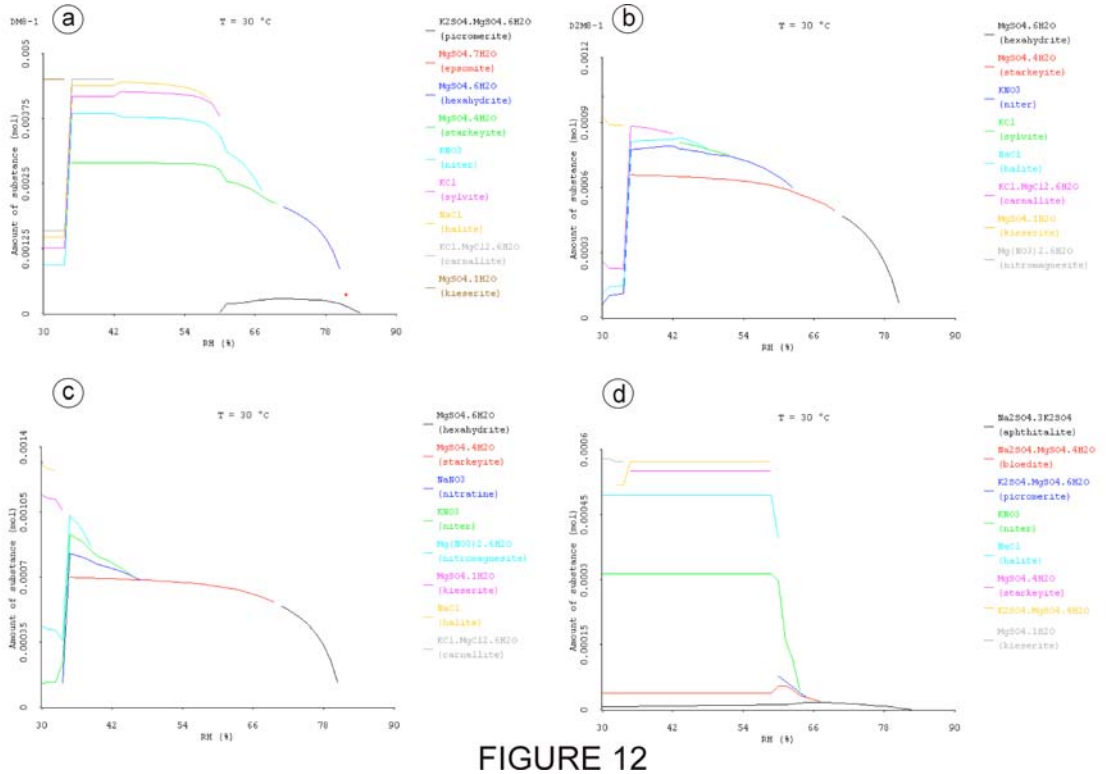
a
T = 30 °C
Amount of substance (mol)
RH (%)
K2SO4.MgSO4.6H2O (picromerite)
MgSO4.7H2O (epsomite)
MgSO4.6H2O (hexahydrite)
MgSO4.4H2O (starkeyite)
KNO3 (niter)
KCl (sylvite)
NaCl (halite)
KCl.MgCl2.6H2O (carnallite)
MgSO4.1H2O (kieserite)
b
T = 30 °C
Amount of substance (mol)
RH (%)
MgSO4.6H2O (hexahydrite)
MgSO4.4H2O (starkeyite)
KNO3 (niter)
KCl (sylvite)
NaCl (halite)
KCl.MgCl2.6H2O (carnallite)
MgSO4.1H2O (kieserite)
Mg(NO3)2.6H2O (nitromagnesite)
c
T = 30 °C
Amount of substance (mol)
RH (%)
MgSO4.6H2O (hexahydrite)
MgSO4.4H2O (starkeyite)
NaNO3 (nitratine)
KNO3 (niter)
Mg(NO3)2.6H2O (nitromagnesite)
MgSO4.1H2O (kieserite)
NaCl (halite)
KCl.MgCl2.6H2O (carnallite)
d
T = 30 °C
Amount of substance (mol)
RH (%)
Na2SO4.3K2SO4 (aphthitalite)
Na2SO4.MgSO4.4H2O (bloedite)
K2SO4.MgSO4.6H2O (picromerite)
KNO3 (niter)
NaCl (halite)
MgSO4.4H2O (starkeyite)
K2SO4.MgSO4.4H2O
MgSO4.1H2O (kieserite)

FIGURE 12